MOTC－IOT－IHMT－CA8908

子波型與波譜型
共關頻振特性比較研究

著者：李勇榮

交通部
運輸研究所 港灣技術研究中心

中華民國八十九年十二月

交通部運輸研究所港灣技術研究中心出版品摘要表

出版品名稱：子波型與波譜型共關頻振特性比較研究

(Wave Characterizations Using Wavelet and Spectral Coherences)

國際標準書號（或叢刊號）	政府出版品統一編號	港灣技術研究中心出版品編號
	009254890340	MOTC-IOT-IHMT-CA8908

主辦單位：海岸工程組
主管：邱永芳
計畫主持人：李勇榮
研究人員：李勇榮
聯絡電話：04-26564216 ext.417
傳真號碼：04-26564216 ext.417

研究期間
自 88 年 7 月
至 89 年 12 月

關鍵詞：wavelet coherences, spectral coherences, the optimum function basis, wave characterizations

摘要：

經由對試驗水槽所取得之水波相關訊號加以探討其波與流（wave-current）或流與流（current-current）共關頻振（coherence）行爲，我們一方面驗証先前相關於水波研究最適化函基 （the optimum function basis）研究之合理性與有用性，一方面則顯示此處共關頻振分析結果其代表性與正確性實乃其來有自、勿庸置疑。

再者此處比較子波型（wavelet）與波譜型（spectral）共關頻振之不同表現與特性。結果顯示，無論是物理行爲解說或是資料分析所需數据量，子波共關頻振之表現均遠遠優於波譜型共關頻振。

具體而言，此文包含的探討子題爲：兩種不同方法其理論背景與內涵本質之物理義意；資料分析長度需求；由巨觀訊號取得微觀之水槽自然頻率及其多模（multi-mode）特性；風波成長階段判別；一些物理現象之表徵、如側頻不穩現象（side-band instability）與史脫克 （Stokes）波特徵；訊號移位變易效應（shift-non-invariant property）探討；非同步或易位量測之影響；虛數與實數子波之不同表徵與用途。

出版日期	頁數	工本費	本 出 版 品 取 得 方 式
89 年 12 月	80	350 元	凡屬機密性出版品均不對外公開。普通性出版品，公營、公益機關團體及學校可函洽本中心免費贈閱；私人及私營機關團體可按工本費價購。

機密等級：

□限閱 □密 □機密 □極機密 □絕對機密

（解密【限】條件：□ 年 月 日解密，□公布後解密，□附件抽存後解密，□工作完成或會議終了時解密，□另行檢討後辦理解密）

■普通

備註：本研究之結論與建議不代表交通部運輸研究所之意見。

PUBLICATION ABSTRACTS OF RESEARCH PROJECTS
INSTITUTE OF HARBOR & MARINE TECHNOLOGY
INSTITUTE OF TRANSPORTATION
MINISTRY OF TRANSPORTATION AND COMMUNICATIONS

TITLE: Wave Characterizations Using Wavelet and Spectral Coherences

ISBN(or ISSN)	GOVERNMENT PUBLICATIONS NUMBER	IHMT SERIAL NUMBER
	009254890340	MOTC-IOT-IHMT-CA8908

DIVISION: Coastal Engineering Division
DIVISION CHIEF: Yuang-Fang Chiu
PRINCIPAL INVESTIGATOR: Yueon-Ron Lee
PROJECT STAFF: Yueon-Ron Lee
PHONE: 04-26564216 ext.417
FAX: 04-26564216 ext.417

PROJECT PERIOD
FROM: July 1999
TO : Dec. 2000

KEY WORDS: wavelet coherences, spectral coherences, the optimum function basis, wave characterizations

ABSTRACT:

Based on an optimum wavelet function basis as explored in several previous studies (Lee and Wu 1996a, b, 1997), the wavelet coherence is shown to yield far much better results than does the spectral coherence. Moreover, the wavelet approach is also shown to be much more economic in the amount of data needed for processing. Through the studies of either wave-current or current-current coherences for both wind waves and Stokes waves, we illuminate many interesting physics related to water waves of wave tank experiments. Specifically, the various topics are: theoretical backgrounds and their inherent implications for both approaches; effects of analyzing data length; the identification of micro features related to the natural frequency of a wave tank; the stage of wind wave development; innate physics and features of instability of Stokes waves; the shift non-invariant property of basis functions; coherence features for non-concurrent or displaced measurements; the different uses of complex and real wavelet coherences.

DATE OF PUBLICATION	NUMBER OF PAGES	PRICE	CLASSIFICATION
Dec. 20, 2000	80	NT:350	☐SECRET ☐CONFIDENTIAL ■UNCLASSIFIED

MOTC – IOT – IHMT – CA8908

Wave Characterizations Using Wavelet and Spectral Coherences

Yueon-Ron Lee

Institute of Harbor and Marine Technology

Decmber 2000

Wave Characterizations Using Wavelet and Spectral Coherences

Yueon-Ron Lee
Institute of Harbor and Marine Technology

Email: ronlee@ms4.hinet.net

Revision: 1.2, December 19, 2000, 23:54:26
Printed: December 26, 2000

LIST OF CONTENTS

LIST OF FIGURES

LIST OF TABLES

内文簡介

本文首先列舉並簡述先前兩篇研究與此處子波共關頻振（wavelet coherence）應用表現之重大關聯，接著我們探討子波型與波譜型（Fourier spectrum）共關頻振的理論背景，說明其由正確解析式轉成具有統計義意之數值求算式當中所引入的不同處理手法及不同的數理本質特性。最後我們以試驗水槽所取得的風波場與机械波場相關訊號研析其各類波與流（wave-current）或流與流（current-current）之間的共關頻振特性。

整体而言，此處分析研究一方面充分驗証先前取得之相關於水波研究用之最適化函基（an optimum function basis）之合理性與有用性；一方面則顯示此處共關頻振分析結果之代表性與正確性實乃勿庸置疑、其來有自。

玆將此處具有獨立子題性質之探討項目或數据分析內容逐項條列如下：

1. 無論在不定性或可判別性上，子波型共關頻振之表現均遠優於波譜型者，且兩者差異甚爲巨大，也因此，子波型共關頻振可以提示多尺度互作用系統下的訊號特性、作用因子、與一些微觀物理行爲等。

2. 子波型共關頻振在分析上所需要的數据量遠低於波譜型者，其差別級距在一個階次（order）以上，此外某些訊息亦很難或無法由波譜共關頻振取得（如後述相關於自然頻率或風波成長細部特徵）。

3. 子波型共關頻振可以由巨觀訊號偵得微觀信息，其一例是由單一組波流信號取得試驗水槽的自然頻率，此外更偵得該自然頻率的多模（multi-mode）性質。

4. 子波型共關頻振可以由單一組波流信號提示風浪相對的成長程度。

5. 子波型共關頻振可以探討一些水波的高階物理本質，如側頻不穩性（side-band instability）、史脫克波（stokes wave）現象、另外亦可提示外加作用因子所引生之細部影響。

6. 子波型共關頻振所受移位導致變易效應（shift-non-invariant property）較小。

7. 除了複數函基子波共關頻振外，實數函基子波共關頻振亦可提供一些不一樣的訊息。基本上實數函基子波共關頻振適合於較非紛紜（relatively less random）或較無瞬變（less transient）之狀況。

8. 詳細列舉造成子波型與波譜型共關頻振之差別表現的各項數理與物理解析因子。

ABSTRACT

Based on an optimum wavelet function basis as explored in several previous studies (Lee and Wu 1996a, b, 1997), the wavelet coherence is shown to yield far much better results than does the spectral coherence. Moreover, the wavelet approach is also shown to be much more economic in the amount of data needed for processing. Through the studies of either wave-current or current-current coherences for both wind waves and Stokes waves, we illuminate many interesting physics related to water waves of wave tank experiments. Specifically, the topics covered are: theoretical backgrounds and their inherent implications for both approaches; effects of analyzing data length; the identification of micro features related to the natural frequency of a wave tank; the stage of wind wave development; innate physics and features of instability of Stokes waves; the shift non-invariant property of basis functions; coherence features for non-concurrent or displaced measurements; the different uses of complex and real wavelet coherences.

Chapter 1

Introduction

1.1 Introduction

Lee and Wu (1996a), using various entropy statistics of transform coefficients, tested among a relatively complete set of discrete Riesz wavelet function bases, as well as Fourier basis, and found the best basis for water wave simulations to be the cardinal B-spline semi-orthogonal wavelet.

In a subsequent paper (Lee and Wu 1996b) they linked the identified discrete Riesz basis to its continuous wavelet transform counterpart related to the modulated Gaussian wavelet and further elaborated on the adaptation of time-frequency windows for better physical implications.

Due to intimate relevances of the two studies to our present interests on wave characterizations through coherence features, the main remarks or primary conclusions of the two studies are briefly outlined in the followings.

Here it is noted that the present study, together with the previous two, on one hand, should justify more than adequately the finding of the optimum bases; on the other hand, should vindicate to an ample extent the various characterizations to be presented in subsequent chapters.

1.2 The optimum Riesz wavelet for water wave studies

The search for an optimum basis started out off the discrete domain. Various unambiguous results were obtained. Notably they were:

1. A vast array of Riesz bases, including orthonormal, semi-orthogonal and bi-orthogonal categories, together with Fourier basis, is tested. These bases include:
   (a) Daubechies most compactly supported wavelets (ONxxA)
   (b) Daubechies least asymmetric wavelets (ONxxS)
   (c) Coiflets (ONxxC)
   (d) Meyer wavelet (Meyer)
   (e) Battle and Lemarié wavelet (B&L)
   (f) Semi-orthogonal wavelets (SOxO)
   (g) Bi-orthogonal wavelets (BOxyO)
   (h) Dual wavelets of semi-orthogonal and bi-orthogonal wavelets (SOxD and BOxyD)
   (i) Wavelet packet best level bases
   (j) Wavelet packet best branch bases
   (k) Fourier basis
2. Entropy criteria based on many settings were adopted (Coifman et al. 1992; Wickerhauser 1992, 1994).
3. Entropy values of all orthonormal wavelets do not fall to the level of non-orthogonal ones.
4. Among all orthonormal wavelets none distinguishes itself from the others, and no clear tendency exists within each basis group.

5. Dual wavelets provide significantly smaller entropy values than as provided by their counterpart wavelets

6. Owing to the same orthonormal nature, wavelet packet bases provide only marginal improvement over their corresponding originating orthonormal wavelet bases.

7. There is little difference in the performances among wavelet packet best branch bases, best level bases, and their originating wavelet bases.

8. The single and far obviously outstanding performer is identified as the dual cubic B-spline semi-orthogonal wavelet constructed by Chui (1992a, b, c). For this basis the probability density function (pdf) of energy distribution shows a complete flatness for 90% of the stretch of the curve, that is to say, literally 90% of the coefficients are null.

9. The important implication of the linear phase filtering property (or symmetry property of basis functions) (Daubechies 1992) is stressed.

10. It is quite certain that there is no need to make any expansion of wavelet construction (i.e., constructing new mother wavelets with longer support length) for any orthonormal basis category.

11. Although the set of transform coefficients of Fourier basis performs significantly better than do those of most wavelet bases, its performance is still not on a par with that of the dual cubic B-spline semi-orthogonal wavelet. In particular, there is big difference between the performances in the $L^1(\mathbb{R})$ space. These have very important implications as the followings. While the $L^2(\mathbb{R})$ space emphasizes the energy; the $L^1(\mathbb{R})$ emphasizes the displacement. And as we also know, energy is related to large scales, whilst signal displacement comparatively puts more weights on smaller scales. Therefore, the pivotal point is that the identified B-spline semi-orthogonal wavelet not only is the better performer when modeling energy phenomena (macro

behaviors) but also is the superior contender in describing fine scale features (micro phenomena or tendencies).

12. In the programming for all the wavelet transforms, as well as their related applications, the Asyst programming language was used, and the programs were written from the ground up so as to fetch maximum flexibility and to cover a widest scope. The code lines amount to about 20,000 lines with many hundreds of modular type sub-programs constructed under an integrated shell program. The programming processes quite often yielded unexpected byproducts as well as rendered further understanding of the theoretical backgrounds. Overall, the back and forth processes resulted a robust analyzing tool that is versatile, automatic, and debugging oriented; henceforth, it rendered the possibility of streamlined and flexible routines that, to out belief, should be relatively error-free for the vast amount of data. Basically, the processes from input of raw data to output of graphs can be batch works.

1.3 The counterpart continuous transform with adaptation in time-frequency windows

The previous section concerns the discrete algorithm; however, without a few additional features that are specific to the continuous wavelet transform, the closeness between the optimum Riesz basis functions and our signals (or their components) will not fulfill its maximum usefulness and the reason for the well performances of the present analyses will also be unclear. Here the notable points are:

1. There is a natural transition from the optimum Riesz wavelet to its continuous wavelet transform counterpart. Incidentally, that continuous wavelet is simply the modulated Gaussian wavelet (Gabor 1946, Aldroubi 1992, Chui 1992a, b, c). This transition fulfills the usefulness of the present methodology by taking advantageous characteristics that are specific to either discrete or continuous wavelet transform.

2. The discrete wavelet transform uses a translation step that is an integer multiple of the dilation scale in the logarithmic measure; whereas, the continuous wavelet transform concerns a translation step that can be as small as the sampling interval for all scales, and the scales can also be specified almost arbitrarily.

3. All the Riesz wavelets handle bases with frame bounds that are either tight or relatively tight; whereas the wavelet used here does not involve frame bounds and might not have frame bounds at all when it is analyzed in the sense of discrete numerics, i.e., it is not even to be qualified as a Riesz wavelet.

4. There is a practical interest in what can be done so as to improve the physical relevance between the basis functions and the wave constituents of our signals. And this is partly realized through the use of adapted time-frequency windows in accord with decaying features of component waves.

5. The relation between the redundancy of wavelet coefficients and the Heisenberg uncertainty principle (Bracewell 1986; Feidhtingger and Gröchenig 1992a, b) is illustrated through the use of the distribution of time-frequency windows over a phase plane (or time-frequency map). And the redundant property of time-frequency windows is one of the key factors leading to the present successful applications.

1.4 Scopes and objectives

When the author embarked the present study, the various concepts stated in the previous sections had not systematically formed in mind, even though numerical results were then in their firm shapes. And I had no slightest idea of how the two studies would contribute. In fact, when I first finished those related to the discrete bases, I was a bit disappointed by the high entropy values provided by all the wavelets other than the seemly most unattractive semi-orthogonal spline wavelet – since at that time I was mostly paying attention to those somewhat fancy wavelets that were more or less finitely supported (i.e., computationally efficient). So, these results were just put on shelf and almost forgotten. Later, when I was working on the continuous wavelet transform, still, I treated it as an independent topic and did not have the thought that there existed a natural transition from its prior study concerning discrete wavelets. And, of course, I was not aware of the fact that there existed multiplying effects due to peculiar properties specific to individual transform. It was when I had done these coherence comparisons that I realized that there had got to be reasons for their performances; I therefore went back to review a few wavelet treatises and gradually gained systematic understandings for the causes.

Just as what was hinted, my study on coherence was essentially an isolated event too. It was when I was reading a paper about coherence characterizations of ocean wind wave fields (Liu 1994), and I felt odd about its definition (or algorithm) of coherence and did not quite agree with the way of its presentations concerning the characterizations. So I liked to clear the puzzles and hoped to find a proper way of coherence processing. Therefore, at any rate, my sole intention was as simple as to see whether I was lucky enough to pick up some byproducts or gain a couple of messages that might possibly relevant to my interests at that time (which is about rain's effects on waves). Nevertheless, to my experience, the most precious results almost always came unexpectedly. I was surprised to find that the wavelet coherence curves behaved so well. In fact, some of the topics even popped up by chance, e.g., the identification of the natural frequency was found by mistakenly feeding my Asyst program with parameters other than my original intention.

Anyhow, let us get to the point to state the relevant parts of the present study. Due to independent nature of individual subject matters, they are arranged topic by topic and each is given a separate chapter unit.

1. Theoretical backgrounds of both wavelet and spectral coherence — the intimacy between the application formulae and their analytic forms will be stated, and individual advantages and shortcomings will be outlined;

2. Effects of data length on the analyses of coherence and the physical significance

thus established;

3. The identification of the natural frequency of an oval tank — the extraction of a micro feature in an overwhelmingly macro energy field;

4. Levels of coherence and the stages of wind wave development;

5. Better innate physics — the Stokes wave views and the water wave instability;

6. Phase effects — a better shift non-invariant property of the used wavelet;

7. Non-concurrent or displaced measurements for both wind wave and Stokes wave cases;

8. Coherences based on complex or real function basis and their different uses;

9. Concluding remarks — summary of factors that lead to the different performances of the two approaches. ❖

Table 1.1: Entropy of orthonormal and semi-orthogonal wavelet coefficients, as well as spectral coefficients, under various statistic criteria.

Wavelet	L**2 coefficient entropy (0 division)	L**2 probability entropy (300 divisions)	L**1 probability entropy (300 divisions)	L**2 probability entropy (200 divisions)	Theotetical dimension (L**2 300 divisions)
B&L	4.691	1.330	3.417	1.179	3.782
Meyer	4.647	1.294	3.365	1.132	3.646
SO3O	4.833	1.669	3.756	1.488	5.307
SO3D	1.823	0.219	1.306	0.172	1.245
Spectrum	2.809	0.270	3.044	0.244	1.310
ON22A	4.993	1.761	3.891	1.516	5.815
ON33A	4.773	1.384	3.499	1.225	3.975
ON44A	4.790	1.517	3.596	1.363	4.559
ON55A	4.819	1.553	3.631	1.367	4.727
ON66A	4.790	1.373	3.456	1.203	3.946
ON77A	4.675	1.355	3.461	1.203	3.877
ON88A	4.645	1.229	3.283	1.082	3.418
ON99A	4.719	1.412	3.501	1.252	4.106
ON00A	4.787	1.423	3.511	1.244	4.149
ON44S	4.835	1.461	3.557	1.281	4.311
ON55S	4.758	1.492	3.576	1.298	4.426
ON66S	4.754	1.402	3.501	1.225	4.065
ON77S	4.751	1.336	3.331	1.188	3.804
ON88S	4.714	1.366	3.481	1.224	3.918
ON99S	4.755	1.469	3.570	1.288	4.345
ON00S	4.635	1.278	3.378	1.134	3.591
ON11C	4.938	1.696	3.832	1.457	5.452
ON22C	4.827	1.468	3.520	1.284	4.342
ON33C	4.756	1.488	3.573	1.333	4.427
ON44C	4.690	1.297	3.337	1.157	3.658
ON55C	4.644	1.309	3.405	1.154	3.703

Table 1.2: Entropy of bi-orthogonal wavelet coefficients under various statistic criteria.

Wavelet	L**2 coefficient entropy (0 division)	L**2 probability entropy (300 divisions)	L**1 probability entropy (300 divisions)	L**2 probability entropy (200 divisions)	Theoretical dimension (L**2 300 divisions)
BO11O	5.395	2.623	4.502	2.299	13.777
BO11D	5.395	2.623	4.502	2.299	13.777
BO13O	4.943	1.806	3.883	1.627	6.084
BO13D	5.266	2.371	4.373	2.053	10.708
BO15O	4.866	1.678	3.755	1.495	5.357
BO15D	5.227	2.291	4.327	1.987	9.882
BO22O	5.282	2.362	4.363	2.083	10.609
BO22D	4.434	1.181	3.284	1.034	3.257
BO24O	4.963	1.862	3.985	1.634	6.438
BO24D	4.359	1.090	3.220	0.962	2.975
BO26O	4.881	1.703	3.835	1.492	5.490
BO26D	4.332	1.064	3.174	0.940	2.899
BO28O	4.857	1.624	3.782	1.452	5.073
BO28D	4.318	1.069	3.157	0.941	2.914
BO31O	5.824	3.174	4.741	2.835	23.894
BO31D	4.377	1.058	2.655	0.936	2.880
BO33O	5.084	2.001	4.062	1.756	7.393
BO33D	4.205	1.102	2.827	0.965	3.011
BO35O	4.850	1.697	3.847	1.506	5.457
BO35D	4.125	1.026	2.776	0.908	2.789
BO37O	4.790	1.658	3.821	1.442	5.247
BO37D	4.106	0.986	2.737	0.873	2.679
BO39O	4.776	1.660	3.835	1.432	5.258
BO39D	4.098	0.967	2.713	0.866	2.629

Chapter 2

Theoretical Backgrounds

2.1 Introduction

Coherence stands for mutual relation or inter-dependency; it manifests an intimacy ranging from a complete clone to a total stranger. For a multi-scale, multi-factor coupling system the levels of coherence among different target quantities represent the phenomena of mutual interaction. By studying variations of coherences under different experimental setups or different input parameters it is possible to identify the evolutions of different scales and to isolate key influencing factors as well as the effects thus associated.

In this study both spectral and wavelet coherences will be used to characterize the scale features of the wave and current fields for various water wave settings. And a few water wave physics will be highlighted.

We note first that, compared with the Fourier coherence approach, the wavelet coherence approach is able to provide far much better information that is not only unambiguous in outcome descriptions but also economical in data amount needed. Various topics to be shown in the following chapters will illustrate all of these. But let us first state explicitly some fundamental backgrounds of the two methods and highlight their respective advantages and disadvantages.

In two somewhat related studies by the author (Lee 1997; Lee and Wu 2000), influences of non-stationary effects or local transient variations were stressed and uncertainties arising from Fourier spectra were further elaborated through the Hilbert transform's viewpoint (Greenberg 1988; Cohen 1995). Herein, additional evidences of the drawbacks imposing upon the Fourier basis functions due to these effects will show up when comparing performances of spectral coherences with those of wavelet coherences.

Apart from the instinctive and fundamental difference between Fourier and wavelet's viewpoints concerning the appropriateness of depicting waves as finitely supported modulating signals, i.e., waves with a life span, there are two other major differences. First, from the viewpoint of their origins, wavelet coherence is a more intimate form of its analytical counterpart than is spectral coherence. More specifically, the wavelet coherence is a direct and natural extension of the wavelet resolution of identity, and therefore involves less artificial intervention. Second, the wavelet coherence is derived from a set of coefficients with an extreme redundancy, while spectral coherence is derived from a set of coefficients associated with orthonormal basis functions. The redundancy provides a fine scale resolution as well as a huge population space needed for coherent statistics, and thus it reduce impacts related to histogram processing, noise effects, a few uncertainty factors, etc (Press et al. 1992, Zhang 1994). Besides, being based on a basis with minimum entropy, the wavelet coefficients possess maximum information contents and lead to clear tendencies in coherent features.

2.2 Spectral coherence

The cross correlation function of two functions $g(t)$ and $h(t)$ is the following inner product $c(t)$

$$c(t) = \langle g(t+\tau), h(\tau) \rangle, \tag{2.1}$$

where τ is a dummy variable. The correlation coefficient function of $c(t)$ is $r_s(t)$,

$$r_s(t) = \frac{c(t)}{\|g(t)\| \|h(t)\|}. \tag{2.2}$$

For real $g(t)$ and $h(t)$, its Fourier transform is

$$\frac{\widehat{c(t)}}{\|g(t)\|\|h(t)\|} = \frac{G(\omega)\overline{H(\omega)}}{\|G(\omega)\|\|\overline{H(\omega)}\|}. \tag{2.3}$$

The artifacts to be introduced in the spectral coherence are associated with the form of expected values and the introduction of a normalization as given by

$$R_s^2(\omega) = \frac{|\mathbf{E}[G(\omega)\overline{H(\omega)}]|^2}{\left(\mathbf{E}[|G(\omega)|^2]\mathbf{E}[|H(\omega)|^2]\right)^{1/2}}, \tag{2.4}$$

where the symbol **E** stands for taking expected value. Since expected values take no action without introducing one more dimension, this equation is identically unity for all frequencies if each data sequence is not segmented and arranged in an array with one additional dimension. The process of this segmentation is completely similar to that commonly implemented in calculating power spectra; its purpose is to reduce the uncertainty or standard deviation of the spectrum. There is no doubt that inherent properties of the discrete Fourier analysis impose similar limitations to the conclusiveness of spectral coherences.

2.3 Wavelet coherence

As to the wavelet coherence, the derivation is even more direct and simpler, along with fewer artifacts.

The wavelet resolution of identity of two functions is

$$\langle g, h\rangle = \frac{1}{c_\psi}\int_0^\infty \frac{1}{a^2}\int_{-\infty}^\infty \langle g, \psi_{a,b}\rangle\overline{\langle h, \psi_{a,b}\rangle}dbda, \tag{2.5}$$

in which c_ψ is a constant and $\psi_{a,b}$ is a wavelet with scale a and translation step b. For a fixed scale a

$$\langle g_a, h_a\rangle = \frac{1}{c_\psi}\frac{1}{a^2}\int_{-\infty}^\infty \langle g, \psi_{a,b}\rangle\overline{\langle h, \psi_{a,b}\rangle}db. \tag{2.6}$$

Here the integration with respect to the translation parameter b is physically, as well as intuitively, similar to the operation of taking an expected value by summing up the elements in the population space. It is therefore quite straightforward to define the wavelet coherence as the natural extension of the normalized equation of resolution of identity:

$$R_w^2(a) = \frac{|\mathbf{E}_b[\langle g, \psi_{a,b}\rangle \overline{\langle h, \psi_{a,b}\rangle}]|^2}{\left(\mathbf{E}_b[|\langle g, \psi_{a,b}\rangle|^2]\mathbf{E}_b[|\langle h, \psi_{a,b}\rangle|^2]\right)^{1/2}}, \tag{2.7}$$

where the subscript b in $\mathbf{E}_b$ stands for taking average with respect to the translation parameter.

It is clear that the wavelet coherence has a more direct linkage to its analytical counterpart than does the spectral coherence.

Unlike the spectral coherence, there is no need to segment the data. The expected values can be obtained in a sense of summing up the results of a simple convolution through a proper imaging and a sign change of the functions and variables involved. Therefore, the population size of the sample space of wavelet coefficients is generally two or three orders of magnitude larger than that for spectral coherence. That is to say, for almost any practical data acquisition scheme and any specific scale, the amount of available coefficients is generally not a concern for the wavelet scheme.

It is also noted here that there are quite fundamental differences between the present approach based on Equation 2.7 and the one adopted in Liu's (1994) paper in which there is no concern for the expected values (and, therefore, it should suffer from the various symptoms related to non-stationary effects).

Still, there is one practical point that facilitates the use of the present wavelet approach. For the wavelet coherence, we can focus only on the portion of scale range that is significant or meaningful to us; but for the spectral coherence, we have no control at all over the frequency range of interest. So a great portion of the spectral results might be entirely irrelevant to our interests. Judging from the fact that for all practical cases we generally only want to, and are just able to, focus on a finite range of scale, we know that the spectral approach wastes resources in the unwanted while the wavelet coherence does just the most right; even though non-orthonormal cases take a much longer computation time. Nevertheless computation efficiency is not our concern.

Again, we note that the basis functions and the associated analyzing scheme used are based on the identified basis discussed in Chapters 1. They are related to the modulated Gaussian wavelet with adaptations in their time-frequency windows. And the wavelet basis function for a scale is

$$\psi_a\left(\frac{t-b}{a}\right) = \pi^{-1/4}\left[e^{-i\frac{\omega_0(a)}{a}(t-b)} - e^{-\omega_0(a)^2/2}\right]e^{-\frac{(t-b)^2}{2a^2}}, \tag{2.8}$$

where the time-frequency window parameter is

$$\text{Erfc}\left[\frac{4}{10}\left(\frac{\omega_0}{a}+2.5\right)-2\right]3+5 = a\omega, \tag{2.9}$$

in which Erfc is the complimentary error function and ω is the carrier frequency based on a characteristic frequency of ω_0. This equation may be modified according to the type of signal studied or according to the frequency range of one's interest. Figure 2.1 shows the curve of the function. The logic for the choice of its constants is self explained in the attached program piece (written in Mathematica programming language). ❖

```
obeg=11.;  oend=5.;
fcenter=2.5;  fdilation=10/4;   fshift=2. ;

perfc=Plot[ Erfc[(1/fdilation)* (freq +fcenter)-fshift]*
                     (obeg-oend)/2+ oend, {freq, -2.5, 8.5} ]
```

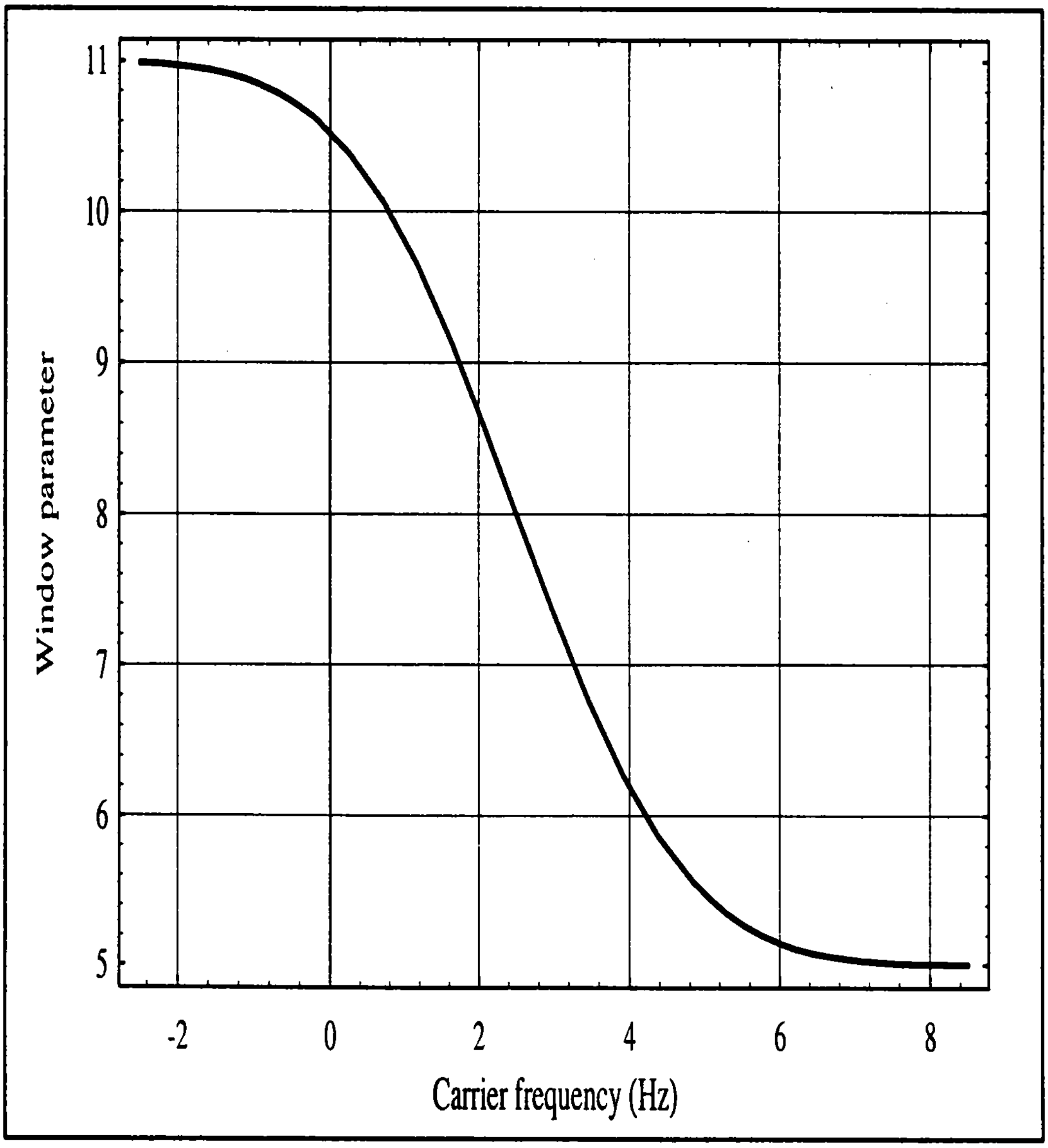

Figure 2.1: The assumed wave decay parameter ω_0 as a function of carrier frequency. The curve can be adjusted according to several parameters: approximate peak frequency, significant range of frequency, range of decay parameter, as well as a curve-shifting adjustment parameter; as are indicated in the attached program piece in Mathematica programming language.

Chapter 3

Experiments

3.1 The oval tank

The experiments were carried out in an oval tank equipped with wind blowing facilities and a mountable mechanical wave generator. Figure 3.1 shows the layout. The circulating oval tank is 31 cm wide and 45 cm high and has a 5-meter straight observational section. The water depth was kept at 24 cm in all experiments. A variable-speed fan was located at the opposite side of the observational section. Horizontal guiding vanes were installed in front of the fan to regulate the airflows, and vertical guiding vanes were installed at the semi-circle tank sections to reduce secondary flows in both air and water. Mechanical waves were generated by the plunger type motion of a wedge controlled by a variable-speed rotor. The whole mechanical construction could be mounted along the observational section.

3.2 The artificial rain simulators

One of the covered topics concerns additional influences due to the external input of rain; therefore, a brief description of the rain simulation follows.

The rain section was composed of two one-meter rain modules (Poon et al. 1992) mounted atop the tank. Hypodermic needles of gauge 23 were uniformly spaced in the bottom of the modules and arranged in an equi-lateral triangular shape with a spacing of 3 cm from center to center. Rain intensity was controlled by the water head above the needle tips.

3.3 The pressure transducer

A differential pressure transducer (Validyne model DP15) was connected to two bottom holes of the tank locating at the upstream and downstream wave gauges that are situated ahead and behind the raining section. The pressure sensor is a typical variable reluctance stress transducer consisting of a diaphragm of magnetically permeable stainless steel clamped between two blocks of stainless steel.

To ensure that no air was trapped in the transducer so that a proper dynamic response could be secured, the transducer was flushed with a long steady water flow through its bleed port and was tilted or shaken somewhat randomly. In addition, a relatively rigid (compared with the magnitude of the pressure concerned) plumbing connection was used, such that effects of low-pass filtering could be avoided. With these due precautions, the small rain-induced stress could be faithfully extracted through the differential water surface displacement.

3.4 The laser Doppler velocimeter

Aqueous flows at several depths in two cross sections along the tank (cf. Figure 3.1) were measured with a laser Doppler velocimeter (LDV). The LDA system is a TSI four-beam, two-component system with two-color, dual-beam backscattering, and counter type signal processor configuration (Adrian 1983). The system is composed of the following main components: (1) fiberoptic transmitting and receiving probe (TSI Model 9115, 9182, and 9140); (2) photodetector and photomultiplier system (Model 9160); (3) frequency shifter with acousto-optic modulator and electronic down-mix module (Model 9180A); (4) signal input conditioner (Model 1994C); (5) fringe timer (Model 1995B); and (6) frequency to analog conversion module (Model 1988). A few auxiliary instruments and accessories were also used in fine-tuning the whole system and in achieving optimum control of data quality, such as: (7) digital readout module; (8) intermittent burst data recording interface; (9) light power meter; (10) fast and sensitive dual channel high-end oscilloscope; etc.

3.5 The waves

Both wind and Stokes waves were adopted. Major wind speeds were 6.0 and 5.1 m sec^{-1}, and the wind was measured with a Pitot tube located 50 cm upwind of the rain section and 11 cm above the still water surface. Stokes waves with wave steepness values of both a relatively small magnitude of 0.06 (weakly nonlinear) and a relatively high magnitude of 0.30 (highly nonlinear) were mechanically generated.

Measurements of water surface displacements were done with the capacitance type tantalum wire probes self-designed by the Air-Sea Interaction Laboratory.

3.6 The Asyst system

In anticipating the difficulties in distinguishing differences incurred by the change of experimental conditions as well as by the short raining section, a highly automated and specially optimized PC-based real time system for both experiments and data analysis was developed using the Asyst programming language. All calibrations, environmental and instrumental noise detections, real-time monitoring, experimental runs, and parts of the on-site near real time-data analyses (such as zero-crossing statistics, displays of raw and filtered sinals, wave height pdf distribution curves, single- or multiple-channel spectral plots, etc.) were done with such a system to ensure maximum controls and peak quality data. ❖

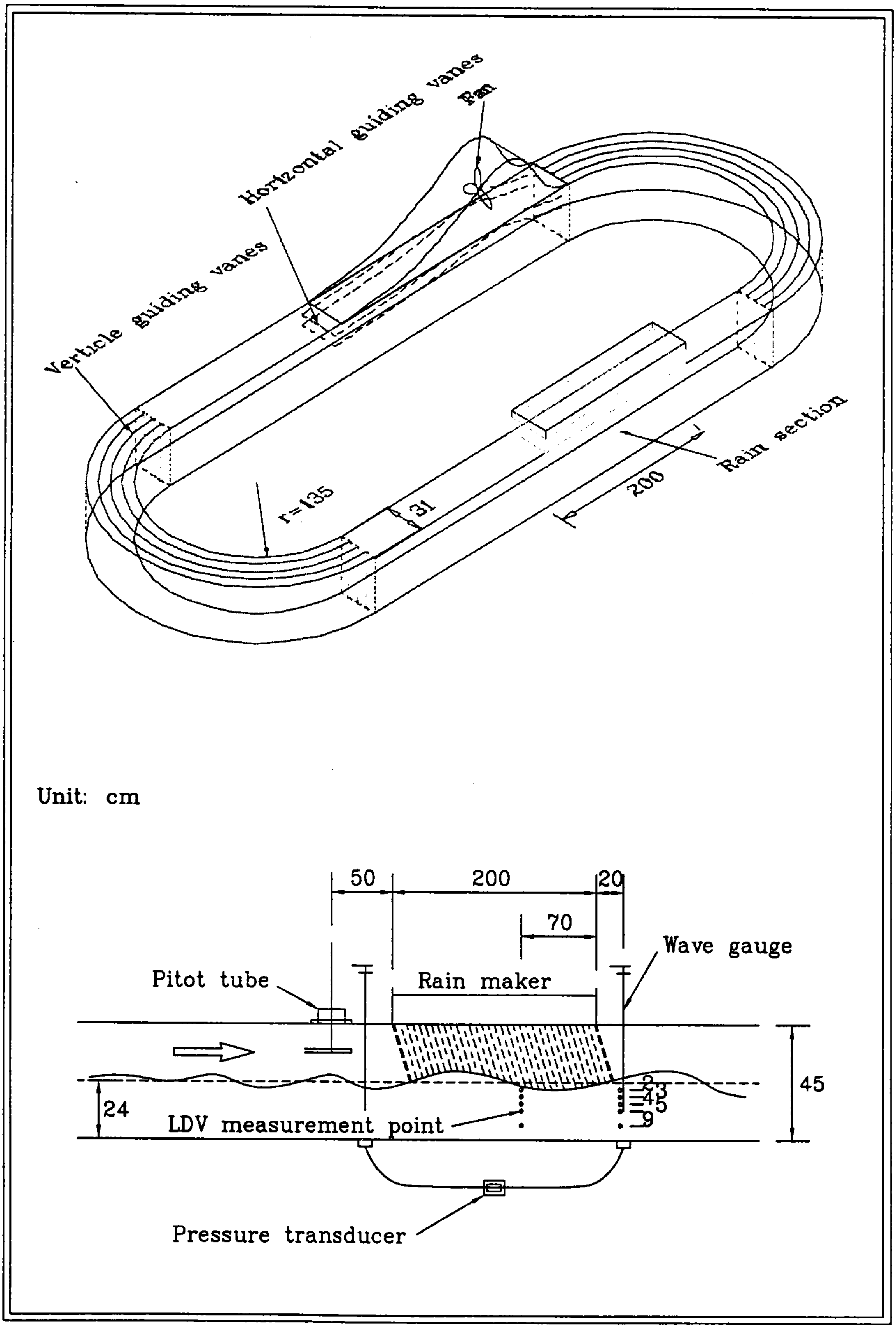

Figure 3.1: Schematic layout of experiment

Chapter 4

Data Length Requirements for the Two Approaches

4.1 Wavelet coherences using different analyzing data lengthes

Both wind-wave (relatively non-stationary from spectral viewpoint, but stationary from zero-up-crossing statistics viewpoint) and Stokes wave (stationary) cases will be used to study the coherent features of the wave and current fields. In this chapter, examples of the wind wave cases are shown. Stokes wave cases to be given in later chapters should also supplement the arguments here.

The wavelet coherences using three different analyzing data lengthes of 1024, 2048, and 4096 points are shown in figure 4.1. In the figure the coherence is between surface wave and aqueous flow and the aqueous flows were measured at individual depths as labeled in the figures. It is seen that various corresponding curves are in extremely good proximities.

It is quite remarkable that the wavelet coherence curves for the non-stationary (either from the Fourier spectrum or the zero-crossing statistics viewpoint) wind-wave cases of 1024-point data length are in quite consistent shapes with those using longer data lengths. Alternatively speaking, increases in the size of population space of wavelet coefficients do not significantly alter the wavelet coherence curves.

4.2 Spectral coherences using different analyzing data lengthes

The spectral coherences using three different analyzing data lengthes of 1024, 2048, and 4096-point are shown in figure 4.2. In the figure the coherence targets and the data source are the same as those of the previous figure. It is seen that little or no proximity exists among various corresponding curves; there are always sharp rises and falls here and there, and detail trends can hardly ever be told. In this perspective, these spectral curves further evidence the various concerns inherent in both the numerical process and the underlying properties of Fourier theory, and also serve as additional illustrations of the questionable direct deconvolution scheme or the problematic blackbox mechanism using an impulse response model as adopted in many studies (Soumekh 1994). Details of these are related to the contents mainly outlined in the introduction chapter (Lee and Wu 1996a, b; and Lee 1997a).

4.3 Spectral coherences using lengthy data and different spectral segmentation lengthes

It is also interesting to note that spectral coherence curves may possibly approximate those of wavelet coherence when an extremely long data length is used. Figure 4.3 shows the spectral coherences using a data length of 9126-point. And the spectral segmentation length is 256- and 1024-point, respectively, for the top and bottom sub-figures.

Although extremely lengthy data may possibly render somewhat compatible tendencies with those of wavelet, the prices are certainly too costly. Besides, in some aspects, a few features can barely be derived as will be given in the following chapters.

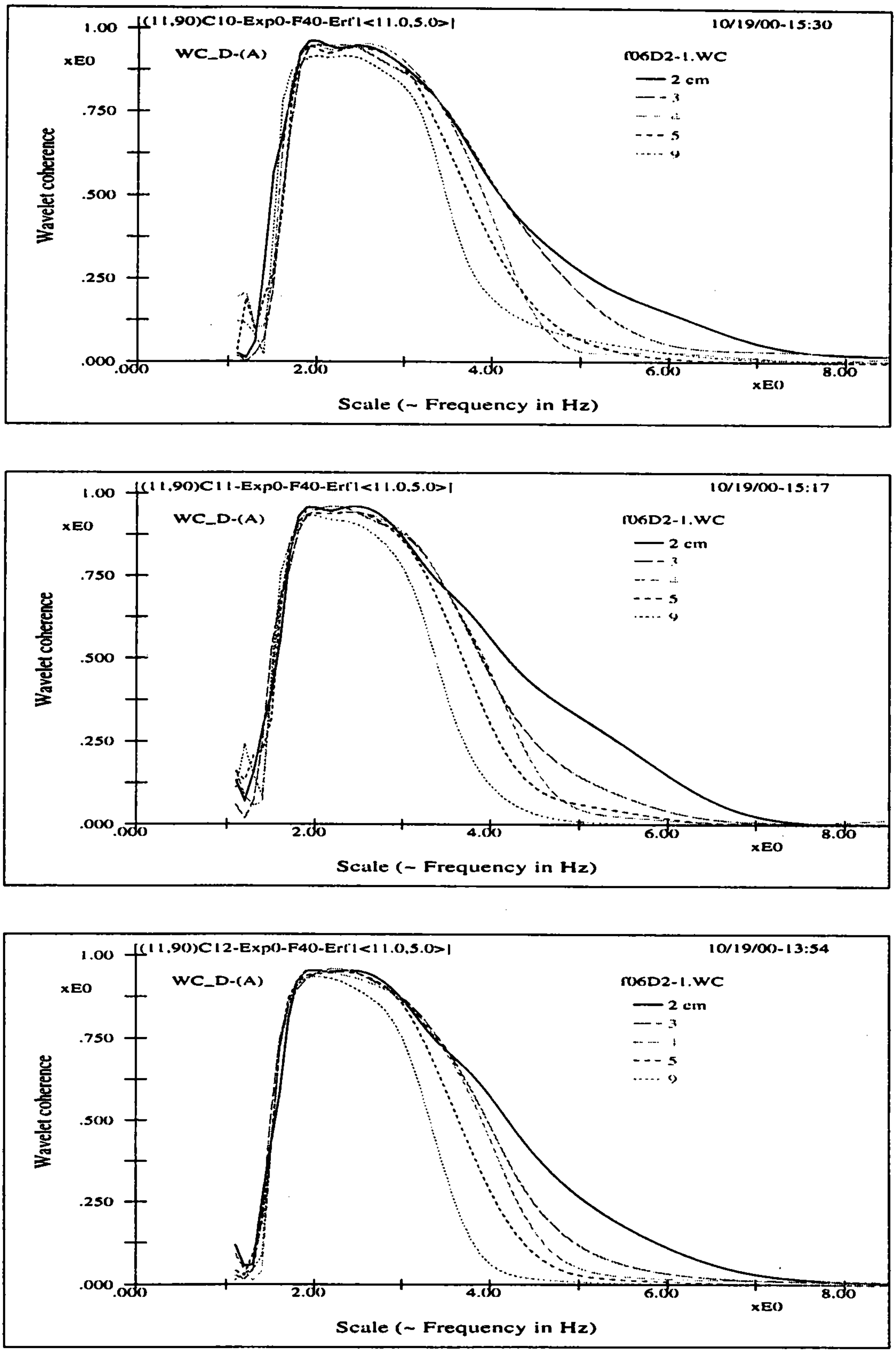

Figure 4.1: The wavelet coherences using three different data lengthes: 1024 `(top)`, 2048 `(middle)`, and 4096-point `(bottom)`. Here the coherence is between surface wave and aqueous flow at each individual depth as labeled in the figures. It is seen that various corresponding curves are extremely good in individual proximities.

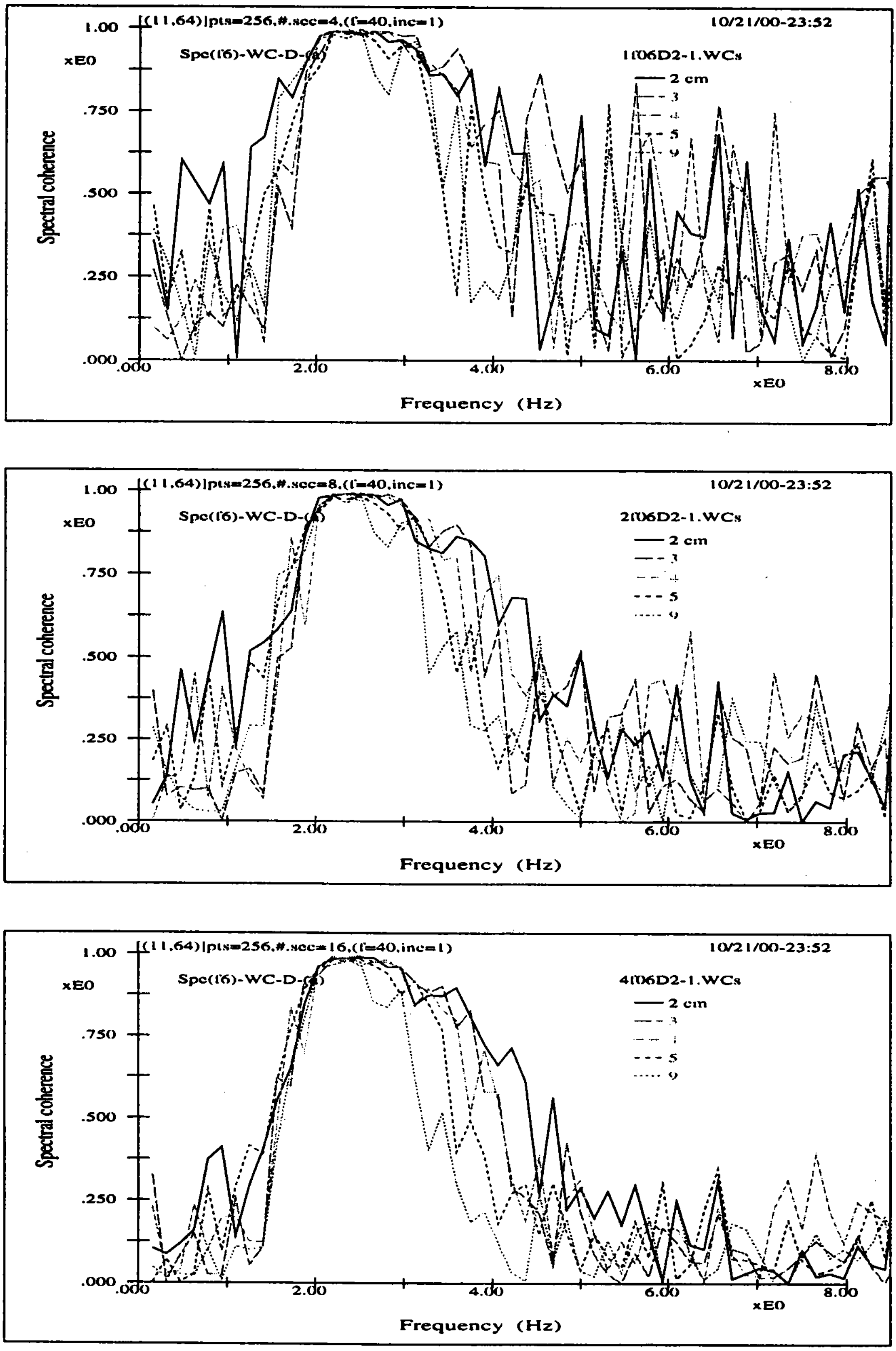

Figure 4.2: The spectral coherences using three different data lengthes: 1024 (top), 2048 (middle), and 4096-point (bottom). The coherence is between surface wave and aqueous flow at each individual depth as labeled in the figures. It is seen that little or no proximity exists among various corresponding curves.

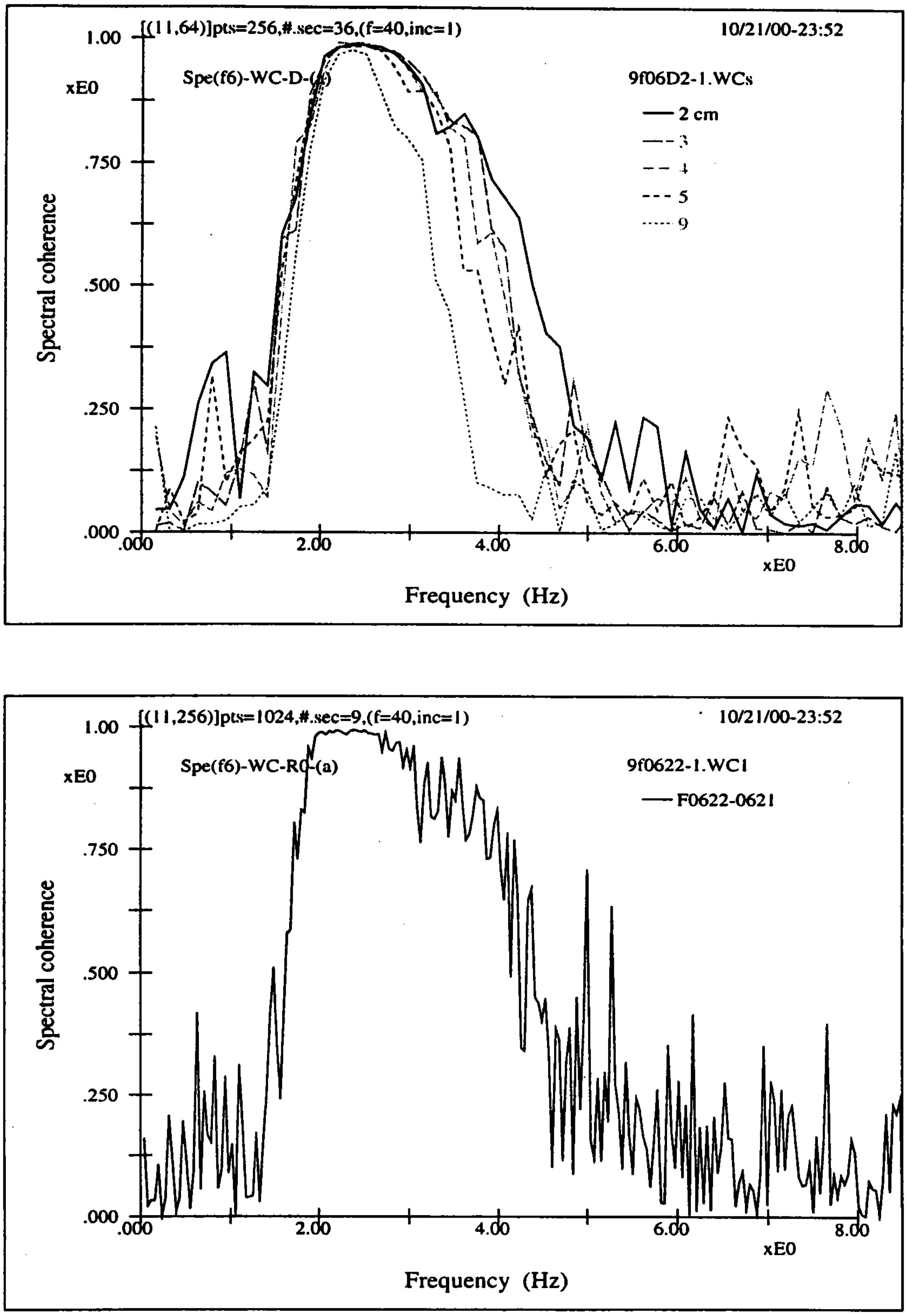

Figure 4.3: The spectral coherences using a data length of 9126-point with different spectral segmentation lengthes. Here the segmentation lengthes of 256 (`top`) and 1024 (`bottom`) points are used, and the coherence is between surface wave and aqueous flow at each individual depth as labeled in the figures. It is seen that spectral results using extremely lengthy data may possibly match those of wavelet, but the tactics might be too costly.

4.4 Informative implications

Overall, additionally, it is not hard to get the following significant implications from the previous figures:

1. Life span of waves — Life spans of component waves are shorter than any analyzing data length used. That is to say, even for the shortest data length of 1024-point the support lengths of all basis functions have properly encompassed all wave components.

2. Stationarity — From the standpoint of the identified wavelet basis, the wave and current fields are reasonably stationary for all data lengthes employed. The truly remarkable point is that the 1024-point data length has almost fulfilled the stationarity.

3. Usefulness of redundancy — The information content of redundancy quickly saturates, i.e., the lengthening of data length provides not much additional information.

4. Length requirements — Combining the three above statements, we see that there is really no need, at least for the present purposes, to acquire lengthy data when the wavelet approach is adopted; this is certainly not the case for the spectral approach.

5. Water wave regularity — Judging from the fact that the function bases of wavelet and Fourier coherences are different, but they yield somewhat similar coherence curves, we regard that our water waves are still relatively quite "regular" when compared with the other wavelet basis functions (Daubechies 1988, 1992; Mallat 1989, 1992, 1998; Coifman et al. 1992a, b, c; Meyer 1992, Press et al. 1992; Massopust 1994).

6. Transient effects and phase ambiguity — The poor performance of spectral coherences is reflected by the rapid variation of the coherent curves as well as the extremely low improvement when the data length is increased. These symptoms

can be attributed to the many causes illustrated in the related studies: such as, the unsatisfactory blackbox mechanism of direct de-convolution; the serious phase ambiguity and local transient effects; the uncertainties associated with Fourier numerics; the rapid diminishing of autocorrelation functions; and the critical changes of transform coefficients due to slight variations of a signal when an orthonormal basis is used. ❖

Chapter 5

The Natural Frequency of the Wind Wave Tank

5.1 A micro feature as identified from macro signals

In this chapter we will see that the wavelet coherence approach is able to identify a micro feature of tiny energy content that should otherwise be invisible. This is illustrated through the extraction of the natural frequency of the wind wave tank using a single measuring pair of the wave-current field.

Figure 5.1 shows the wave-current coherences for currents measured at two individual depthes, and the frequency range is from almost zero to 2.0 Hz. The existence of the somewhat regularly repeated bumps at the lower end of the coherence curves has its own physical significance associated with the natural frequency of the tank as to be supplementally explained in the figures that follow. We note that the irregularity for the left-most bump is caused by the long life span of the natural frequency. At this scale range the support lengthes of wavelet basis functions are unable to cover the whole span; therefore edge effects are introduced.

The remarkable truth here is: not only the wavelet coherence is able to extract a component signal of relatively tiny energy content (less than $1/10,000$ of that of the primary wave), but also it is able to identify the harmonic feature of the embedded micro signal.

Figure 5.2 show the raw wind wave signal used to derive the above natural frequency.

It is quite certain that the natural frequency as well as its features can hardly ever be perceived with any other numerical tool.

5.2 Additional evidence as provided by a noise signal of nearly null content

In this section additional evidences of the existence of the natural frequency are provided using different types of signal. Figure 5.3 shows a signal of almost null content. The signal is basically just a noise of instrument origin superimposing upon a background natural frequency wave. It was acquired after stopping the blowing wind. With the ceasing of wind the water surface was visually seen to calm down immediately, but, due to the relatively long wave nature of the natural frequency, the natural frequency wave kept on propagating, and the acquired signal is therefore a noisy signal with the natural frequency wave embedded.

Here the natural frequency wave is extracted in two ways: One is by filtering in a maximum extend the noise signal. The other is by calculating the auto-correlation function of the somewhat filtered noise signal with a zero offset. The dotted line in Figure 5.3 shows the maximally filtered signal. Figure 5.4 shows the auto-correlation function. The period of the natural frequency is clearly seen to be about 13 seconds. The tapering of the auto-correlation curve is mainly due to zero padding adopted in the numerical processing.

Additionally, figure 5.5 shows a raw signal of relatively low noise obtained by the sensitive differential pressure transducer. The instrument faithfully recorded the tiny water head difference between the two sections and revealed a few properties of the wave.

Again, even for the extreme smallness of wave steepness for this natural frequency wave, the wave type is more of a Stokes wave with flatter troughs and sharper peaks, which in turn yield slower rises and steeper descends of differential pressures as shown in the figure.

In contrast, figure 5.6 shows that the power spectral curves of the noise signal. Here we

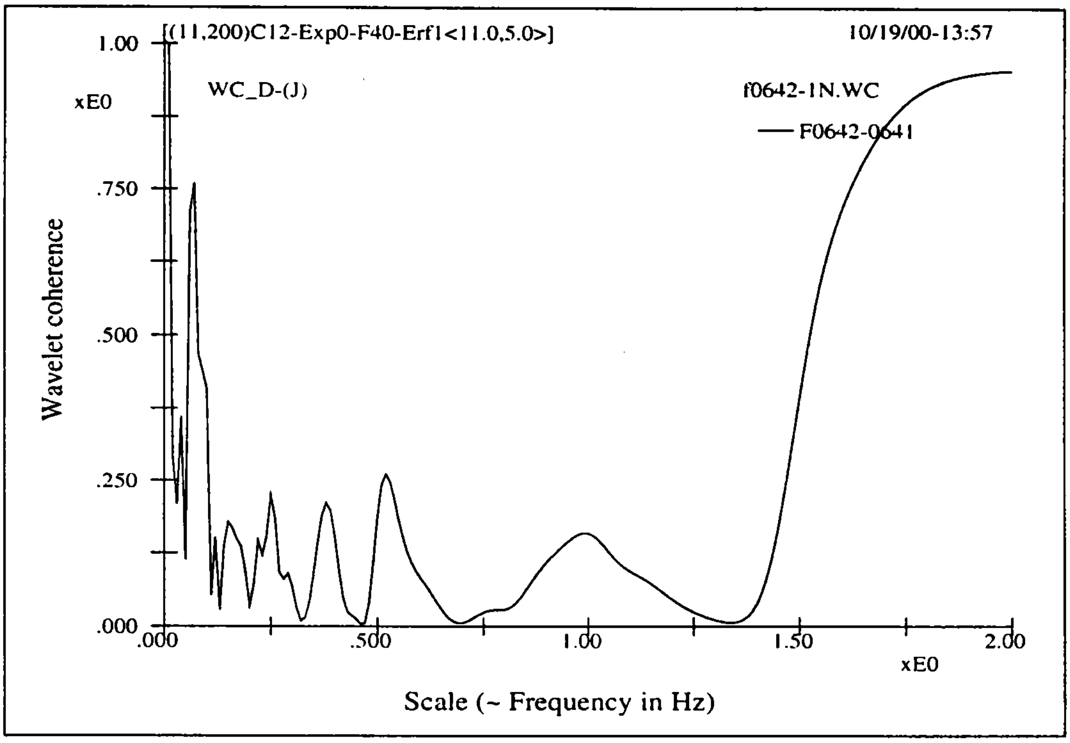

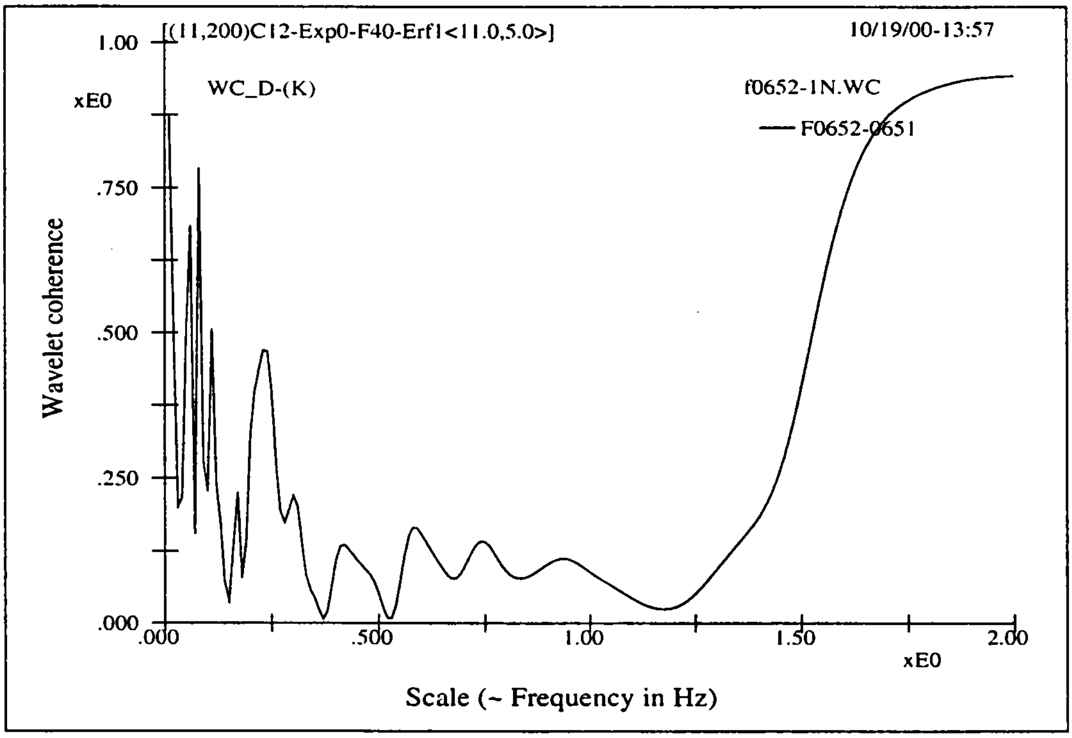

Figure 5.1: The feature of the somewhat regularly repeated bumps at the lower end of the coherence curve has its own physical significance associated with the natural frequency of the tank. It is quite remarkable that wavelet coherence is able to extract component (or embedded) signal of energy content of less than $1/10,000$ of that of the primary wave and even to tell its harmonic feature.

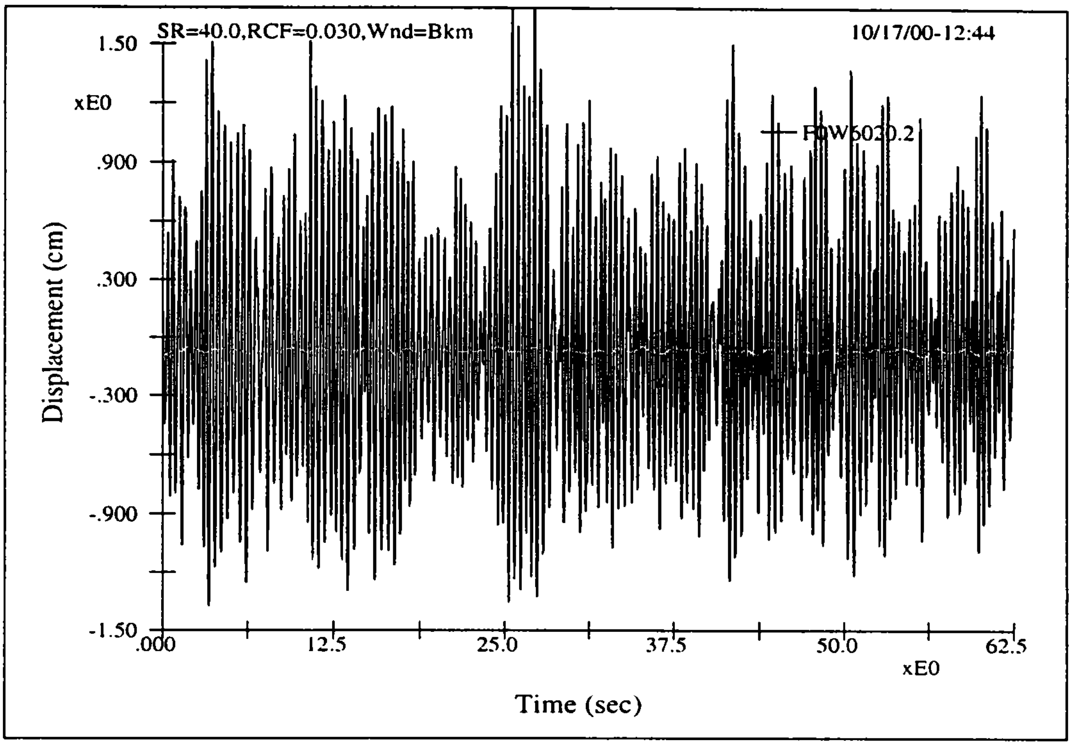

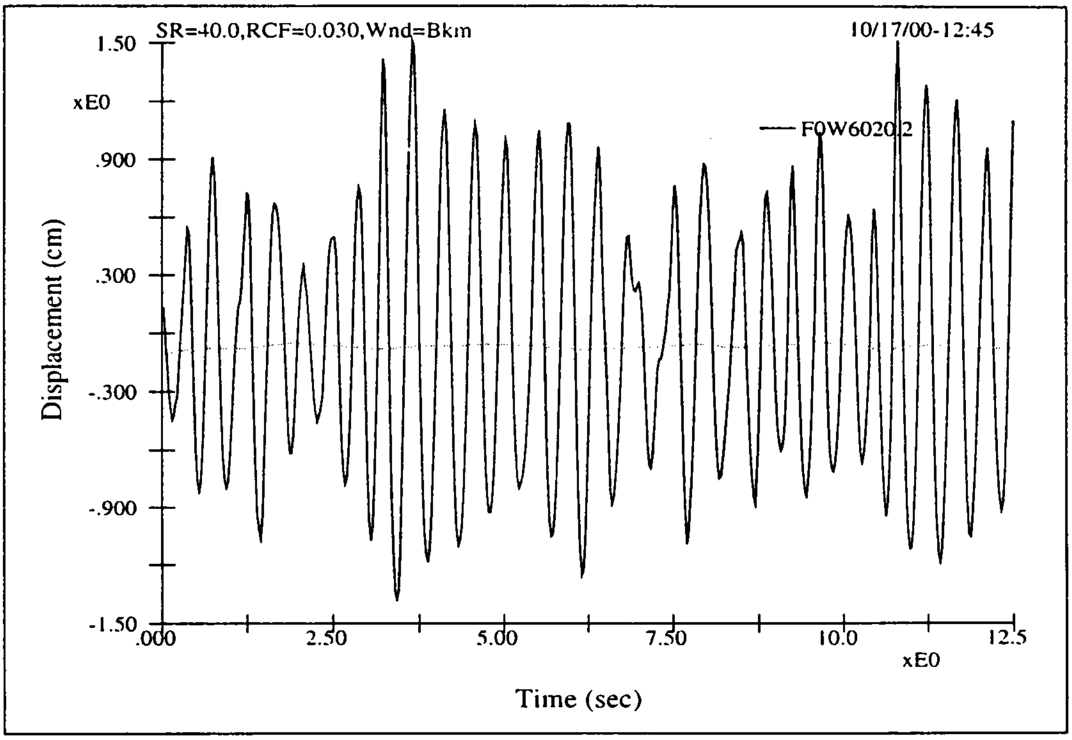

Figure 5.2: The raw wind wave signal that is used to derive the natural frequency – to the author knowledge, the micro feature can hardly ever be told by any other mean.

have no easy identification of the natural frequency even though, analytically, power spectrum is the Fourier transform of the auto-correlation function. This should be attributed to the many side effects of the numerical process as well as the nature of the Fourier basis functions. Understandably, either spectral coherences or power spectral curves are unable to tell the existence of the natural frequency, not to mention the multi-band nature associated with a Stokes wave (Lamb 1932). ❖

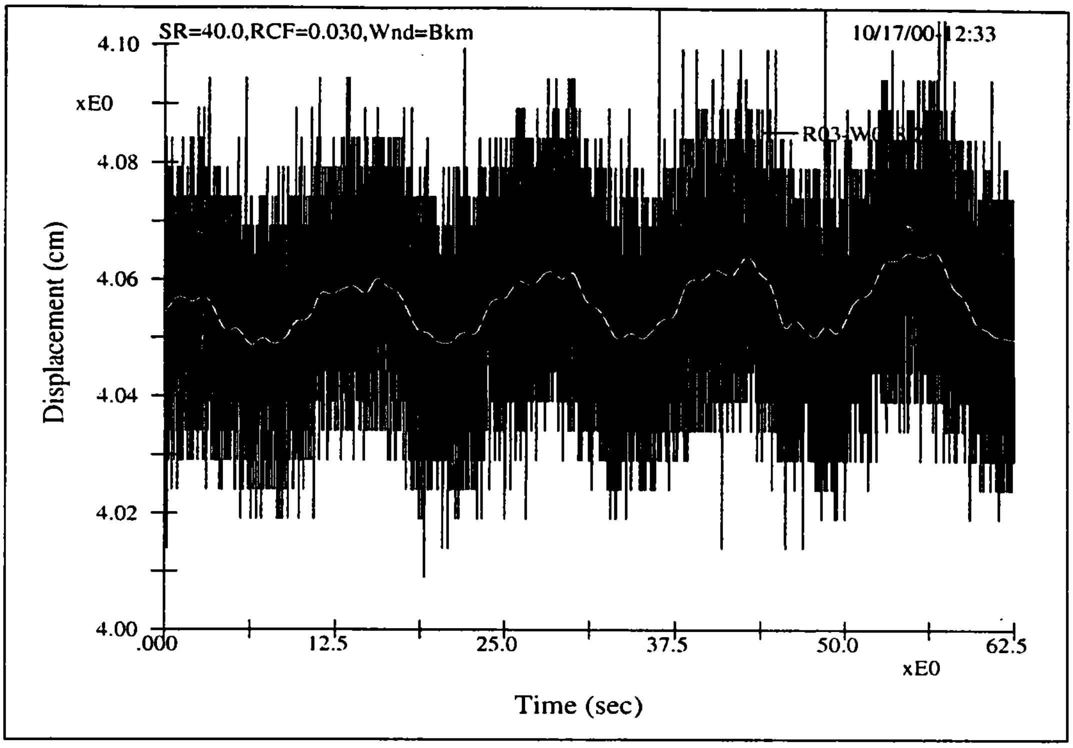

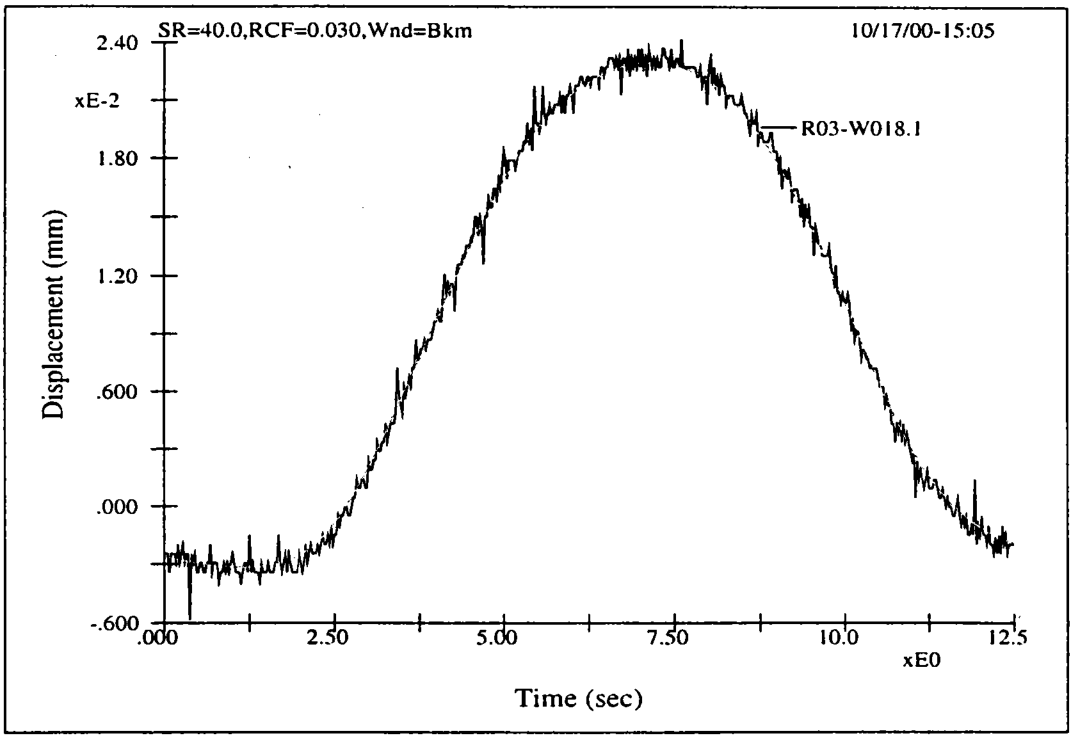

Figure 5.3: A signal of nearly null content (top) serves as an additional evidence for the existence of the natural frequency. While the almost null wave gauge signal of mainly noise content is hard to tell the existence of the natural frequency without special attentions, the low-noise pressure transducer faithfully recorded the tiny water head difference (bottom). These signals were acquired soon after the blowing wind was stopped and the water surface was visually without waves.

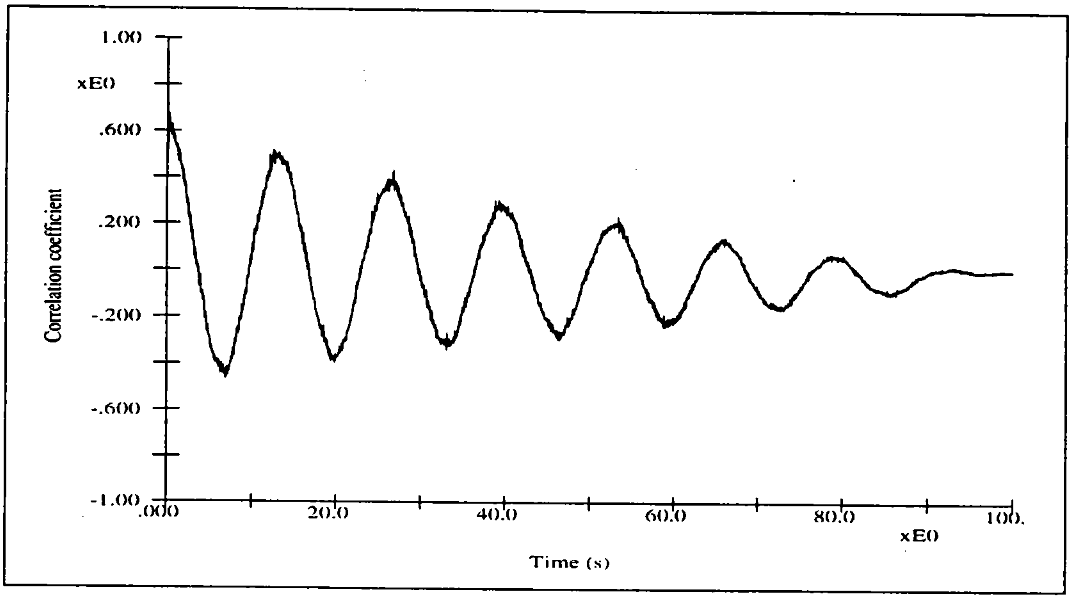

Figure 5.4: The auto-correlation coefficient function of the noisy wave form (the top sub-figure of figure 5.3) shows a few characteristics related to the natural frequency of the oval tank. The tapering of the curve is mainly due to zero padding of the numerical process. The slower rises and steeper drops of the curve is compatible with the measurement of the differential pressure transducer.

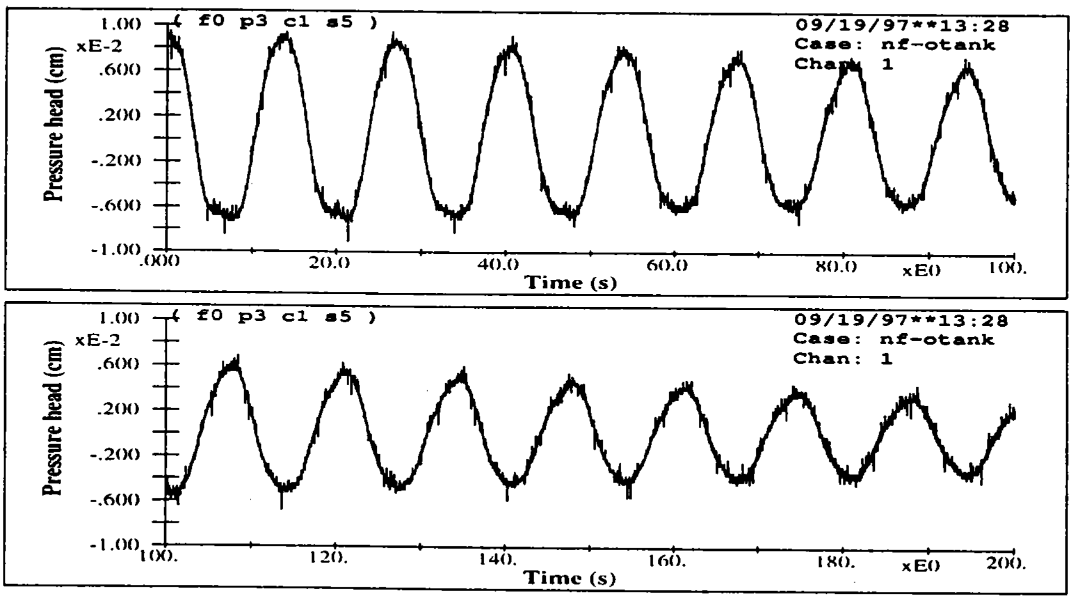

Figure 5.5: The raw signal of the pressure transducer also clearly reveals the natural frequency wave. Even for the extreme smallness of wave steepness, the wave is seen to be more like a Stokes wave with flatter troughs and sharper peaks, which in turn yield slower rises and steeper descends of differential pressures as shown in this figure.

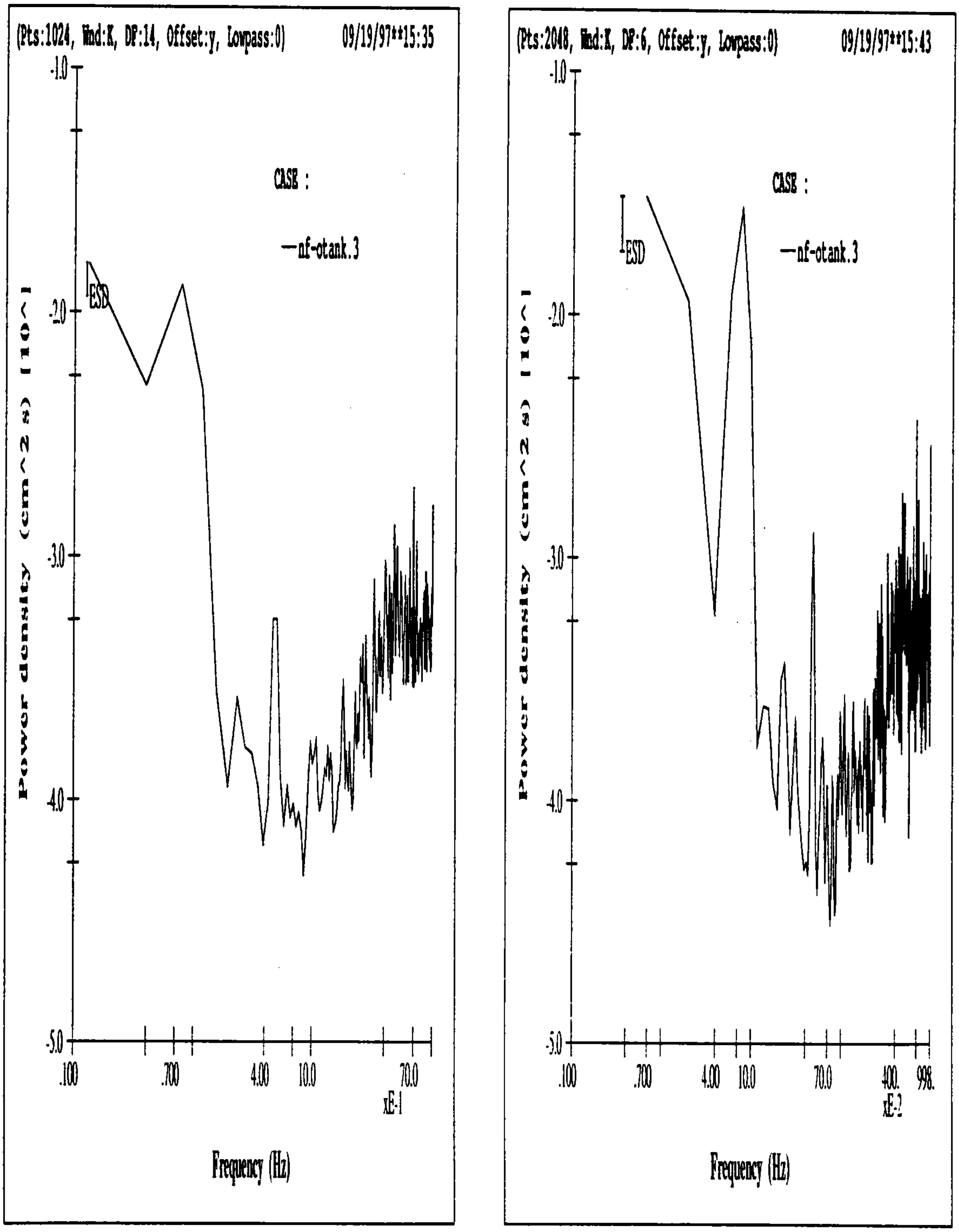

Figure 5.6: The power spectral curves of the noise signal — there is no easy identification for the natural frequency. Though, analytically, power spectrum is the Fourier transform of the auto-correlation function, side effects of the numerical process cause ambiguity and render the judgement a bit difficult. It is quite certain that these curves are not able to yield multi-band nature of the natural frequency related to a Stokes wave.

Chapter 6

Coherences and the Stage of Wind Wave Development

6.1 Coherence and relative energy

Coherence is a normalized value, within a coherence curve, higher coherences are associated with components of relatively higher energy content. In this chapter we will see that wavelet coherence is able to differentiate intricate details and also shows that the wavelet coherence levels are able to indicate the relative maturity of interaction under different wind conditions. In this regard, the spectral coherence is generally only capable of showing mediocre tendency for a single coherent curve.

6.2 Coherence and the maturity of wind wave

Figure 6.1 shows wave-current coherences for current measurement depthes at 2 and 5 cm below the still water surface and wind speeds of 6.1, 5.1 and 4.0 m s^{-1}. It can be seen that the levels of coherence show the individual stages of wind wave developments. A few explanations are:

- Since various data for the figure were all sampled at the same location along the tank, the relative levels of coherence signify different maturity of wind wave development. With the increase of wind speed it is seen that the peak of the coherence curve shifts towards the upper left corner of the graph, i.e, the trend of peak frequency getting lower and peak coherence getting higher. Such indications of maturity can also be verified by measuring a second wind wave signal at a downstream (or upstream) location and then comparing the statistical difference between the two.

- The maturity is also indicated by the developments of both long and short component waves for cases of aqueous flows measured at a shallower measurement depth of 2 cm. For high wind speed, the curve at high frequency end does not extent as to the right as does the low wind speed; this is due to the higher instability (or randomness) of the wave-current fields. For its lower frequency end, the curve is also seen to shift to the left significantly.

- Since shorter waves do not penetrate as deep as longer ones, the parts of different coherence curves at the high frequency end for the deeper measurement depth of 5 cm are seen to close to each other and not to extend as to the right as do those of measurement depth of 2 cm. This is an indication of the maturity of short wave components. However, at the low frequency end, coherences for the higher wind speeds are seen to shift further towards the left hand side as compared with those of measurement of 2 cm depth, but this does not happen for the smallest wind speed.

- As indicated in figure 4.2 it is generally not possible to differentiate the coherence levels using Fourier spectral approach since the peaks of the curves (corresponding to wave components with somewhat significant energy) are saturated with a value of unity. Besides, all the features stated above are not as clearly identifiable as those of wavelet coherences. ❖

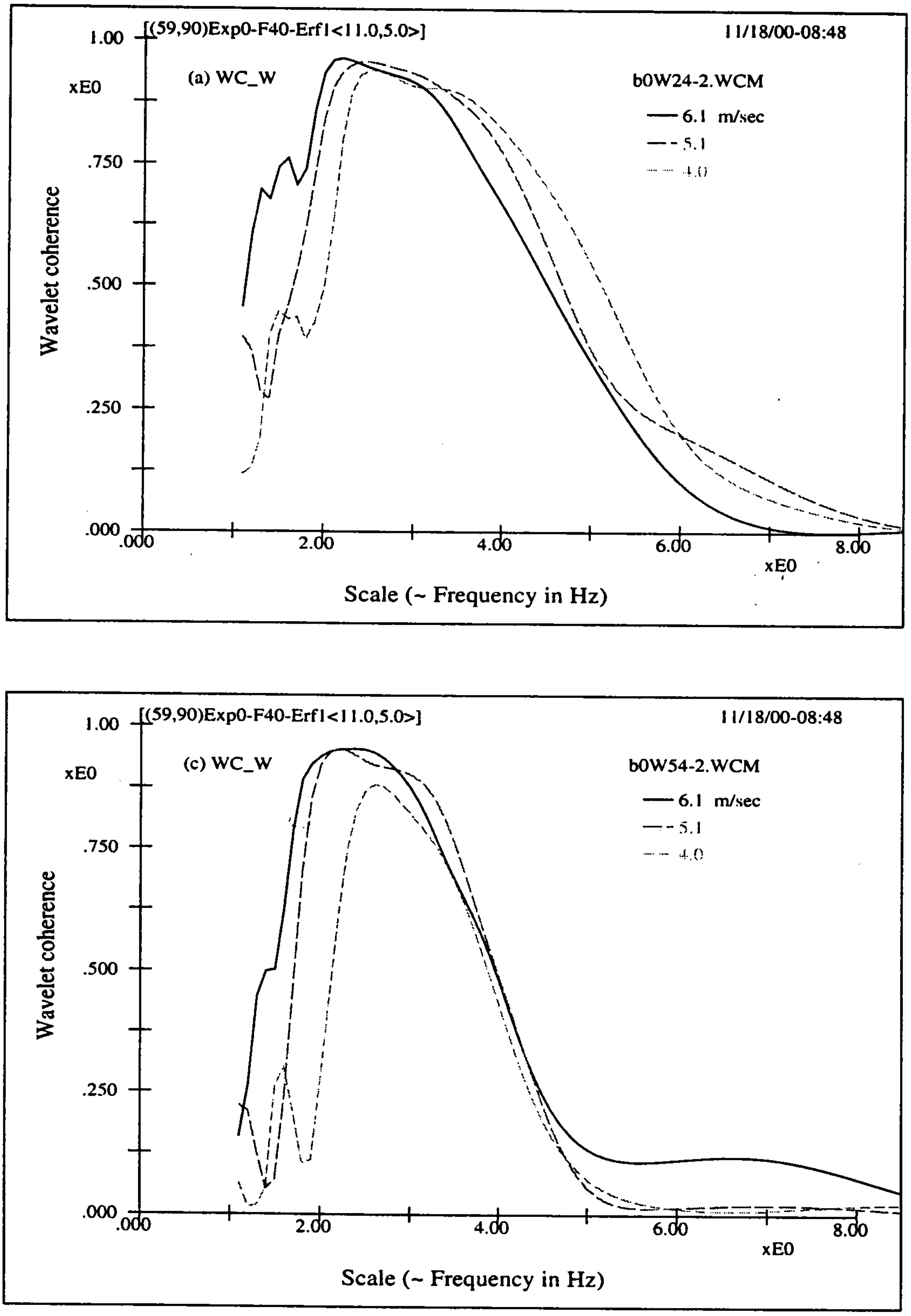

Figure 6.1: Higher coherence is associated with relatively higher energy content – the wavelet coherence is able to indicate the maturity of wind waves. Here wave-current coherences at depthes 2 cm (top) and 5 cm (bottom) for three different wind speeds as labeled in the figures show the individual stages of wind wave development.

Chapter 7

Coherence and the Instability of Water Wave

7.1 Introduction

In this chapter we study coherence features of different Stokes waves with different wave steepness values and show that wavelet coherence features are able to indicate phenomena related to water wave instability. But first let us briefly state a few concepts related to water wave instability.

7.2 Stokes waves with different wave slopes

The stokes waves were generated using a plunger type mechanical wave maker consisted of a triangular wedge pedal and driven by a variable-speed rotor. The representative values of wave steepness of the Stokes waves are estimated from the wave slopes of individual fundamental harmonics. And amplitude modulations of individual harmonic components are derived from the Hilbert transform method (Lee 1997).

Figure 7.1 shows the power spectral curves of two Stokes waves with wave steepness values of 0.06 and 0.30 for individual fundamental harmonics. Figure 7.2 shows the amplitude modulations of the first four harmonics for the Stokes wave with the 0.06 wave steepness. For this Stokes wave the instability is relatively quite minor.

The high instability is illustrated through the use of the Stokes wave with the representative wave slope of 0.3. Here the evolutions of time-frequency (or time-scale) phase planes at three measurement locations along the tank (2.3, 3.5 and 3.6 meters, respectively, away the wave generator) are shown in figure 7.3. For his case the peak frequency for the fundamental harmonic is about 2.7 Hz.

In the figure the Fermi-Pasta-Ulam (FPU) recurrence phenomenon (Hasselmann 1962; Brooke Benjamin 1967; Brooke Benjamin and Feir 1967; Lighthill 1967; Brooke Benjamin and Mahony 1971; Yuen 1975; Longuet-Higgins 1978a, b; Stuart and DiPrima 1978; Debnath 1994) was compatibly characterized with underlying theory for having a cutoff instability bandwidth of 2.0 Hz and an instability development time of 0.65 s. Additionally, a few illuminating points are: (1) The wiggling of the dark frequency band strongly indicates the existence of constant swapping of energy among different frequencies and shows a typical feature of instability. (2) When the wave evolves down the tank, The relative contrasts of dark spots within sub-figures are getting darker and localized. (3) There is downward expansion of frequency band when the wave evolves down the tank, as is seen by comparing the bottom parts of individual sub-figures – the bottom parts of the time-scale planes are getting darker and there seems to be a somewhat regular pattern evolving when the wave propagates downstream. In general, these features are consistent with the findings of several previous studies (Whitham 1967; Lake and Yuen 1977; Lake et al. 1977; Su 1982; Melville 1982, 1983).

7.3 Coherence and the instability

The wavelet wave-current coherences for the two Stokes waves of wave steepness of 0.06 and 0.30 are shown in figure 7.4, and the corresponding spectral coherences are shown in figure 7.5.

For the low wave slope of 0.06 the coherence peaks for the fundamental harmonic bands are close to unity for all depthes and the curves are also near to each other; for the

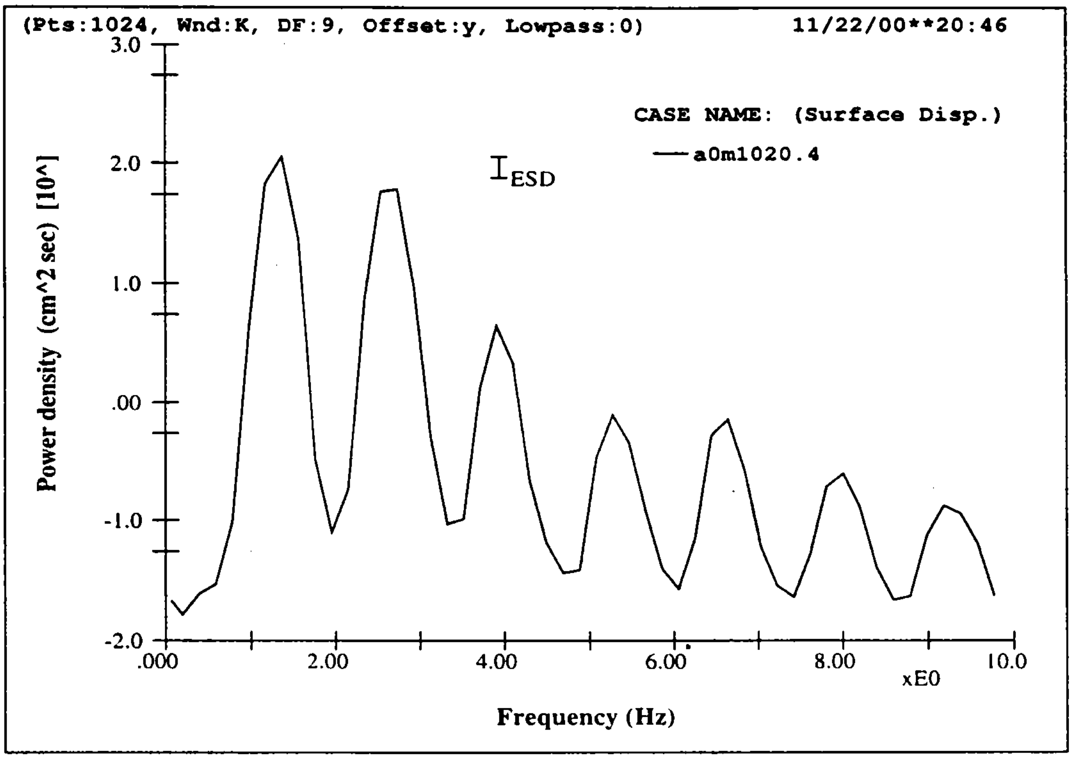

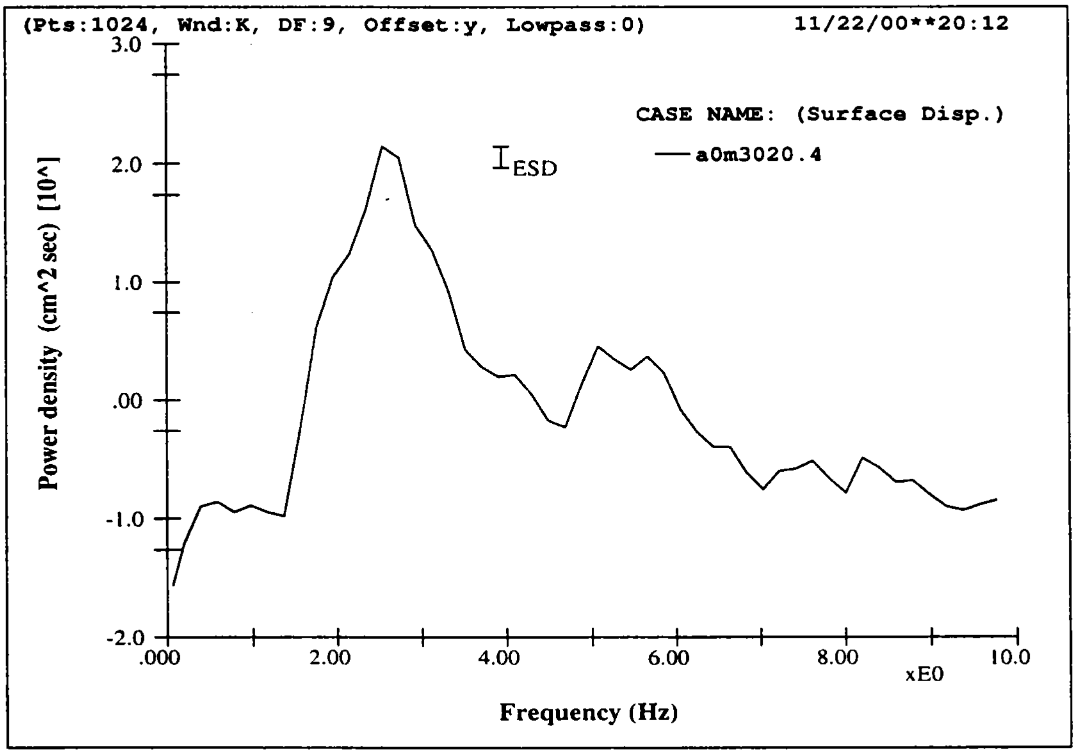

Figure 7.1: Power spectra of Stokes waves with different inherent instability — The wave steepness values are 0.06 (`top`) and 0.30 (`bottom`) for individual fundamental harmonics.

second peak (second harmonic), due to shorter wave length and higher local wave slope, the peak values are lower and the curves are not as close to each other as what the first peak shows. Nevertheless, both peaks generally indicate features of low instability.

For the high wave slope of 0.30 the coherence levels for individual curves are seen to departed substantially from each other; moreover, it is seen that their coherence levels are reduced when compared with those of small wave steepness and that the deeper the depth the lower the coherence. Here the reasonable explanation is the downward expansion as well as the localized effects of low frequency band, as shown in figure 7.3.

As to the spectral coherence curves shown in figure 7.5, once again, we get further ideas of how difficult it is to gather any informative physics. ❖

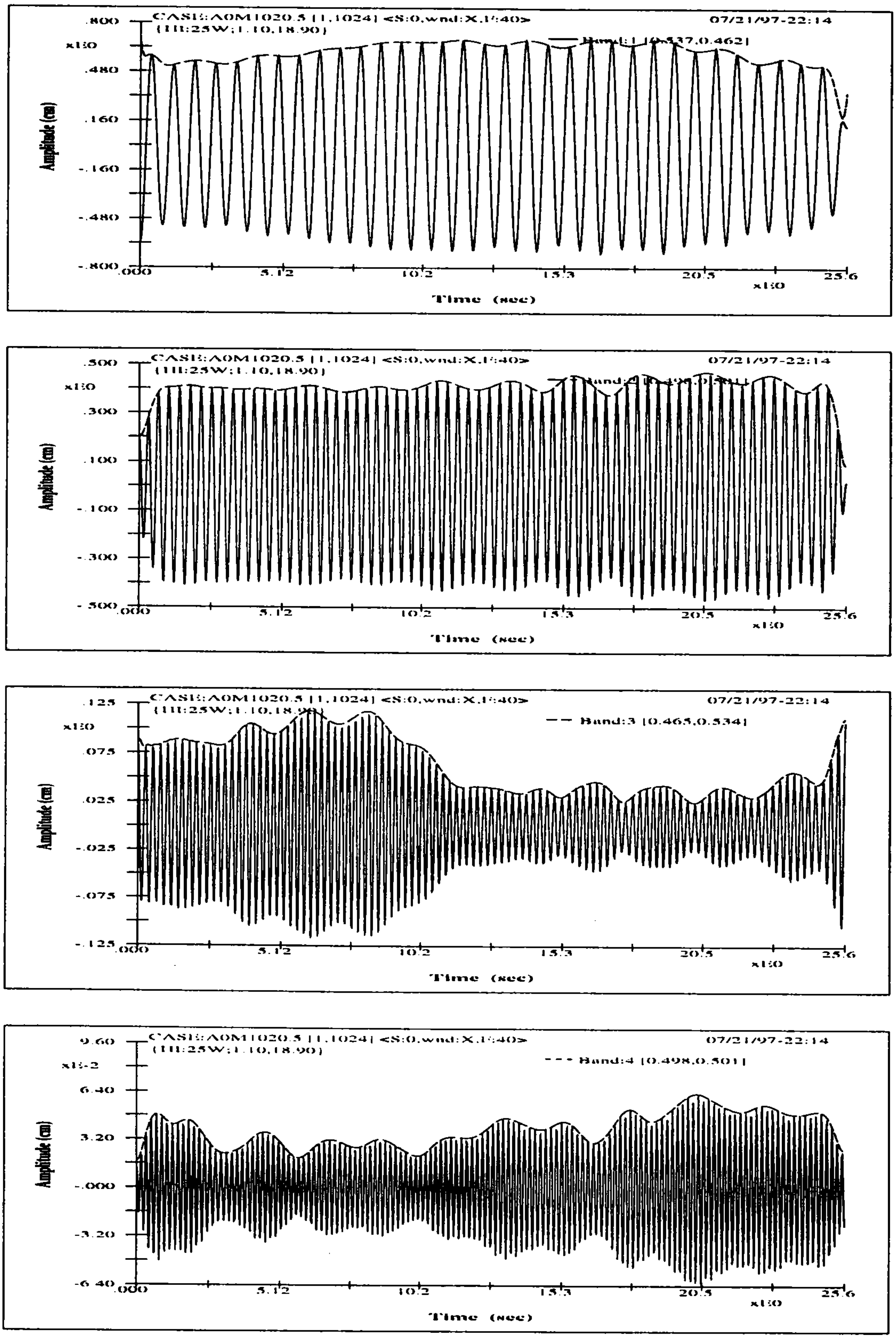

Figure 7.2: The harmonic components and their amplitude modulations for a Stokes wave having a 0.06 wave steepness for its fundamental harmonic.

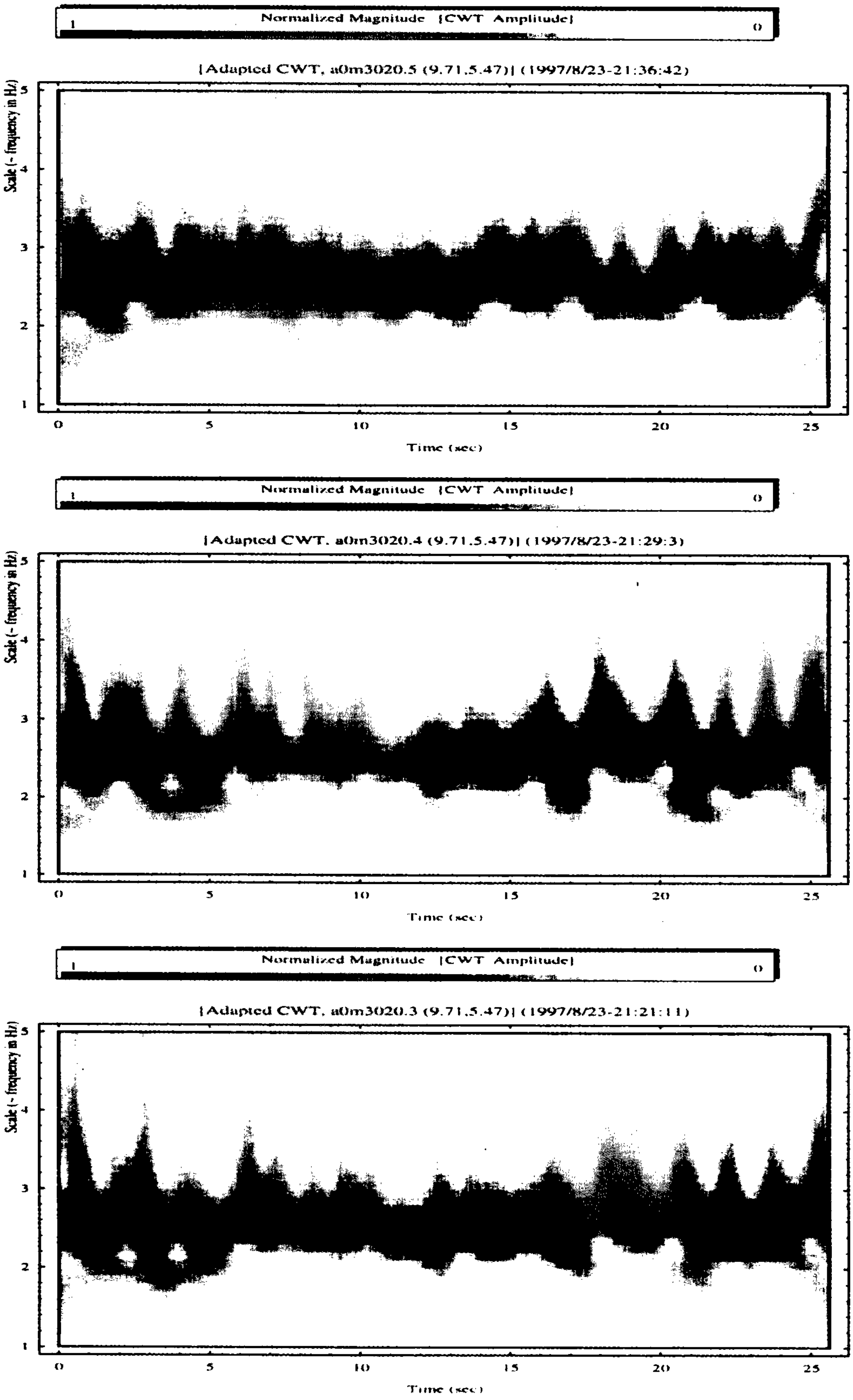

Figure 7.3: Evolutions of time-scale phase planes for a Stokes wave with a fundamental harmonic of 2.7 Hz — Representative values of ka are about 0.30. The top sub-figure is for station 2.3 meters away the wave maker; the middle sub-figure is for 3.5 meters away; and the bottom for 3.6 meters. Features of the plots reasonably identify both qualitatively and quantitatively the characteristics related to the water wave instability or FPU recurrence phenomena, as are explained in the text.

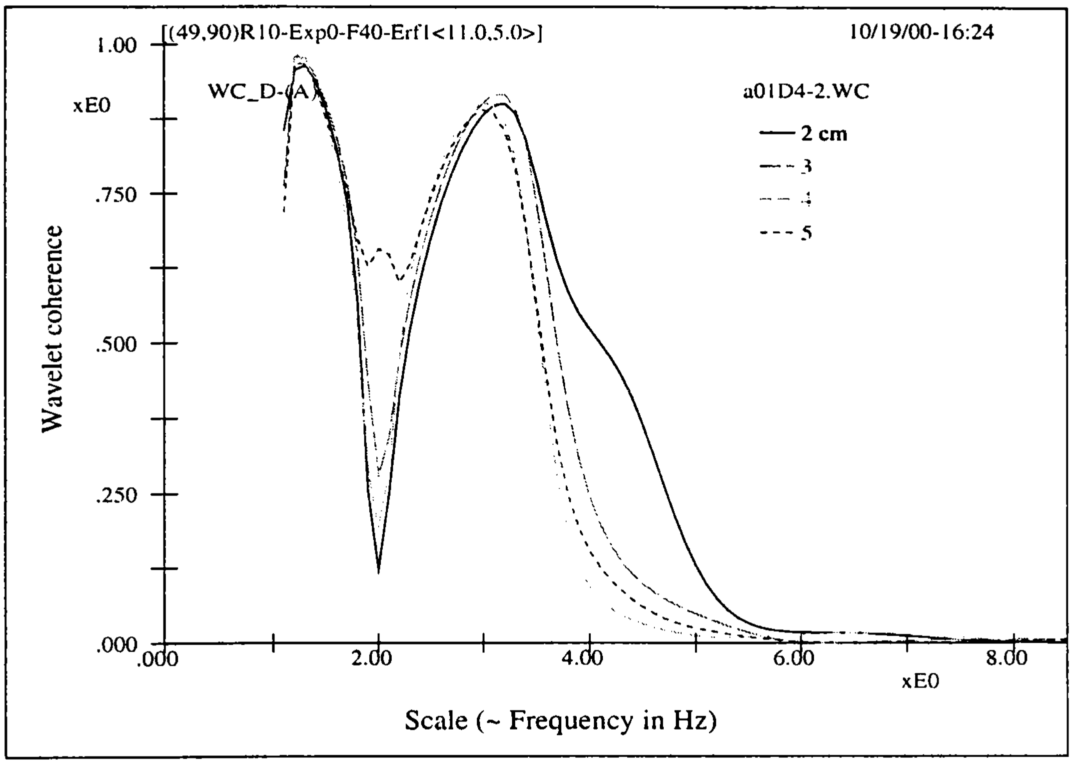

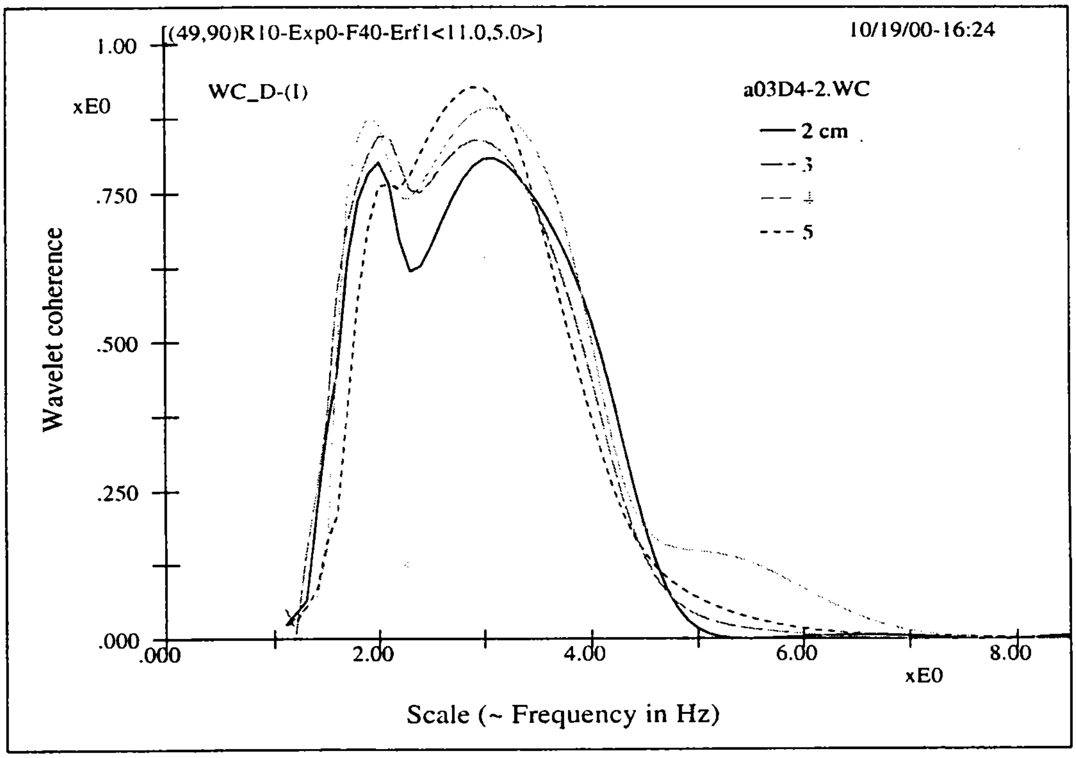

Figure 7.4: The wavelet wave-current coherences for two Stokes waves with wave steepness values of 0.06 (top) and 0.30 (bottom) —The wavelet coherences are seen to indicate different instability features associated with different wave slopes, either from the levels of coherence or from the changes of coherence curves with different depthes.

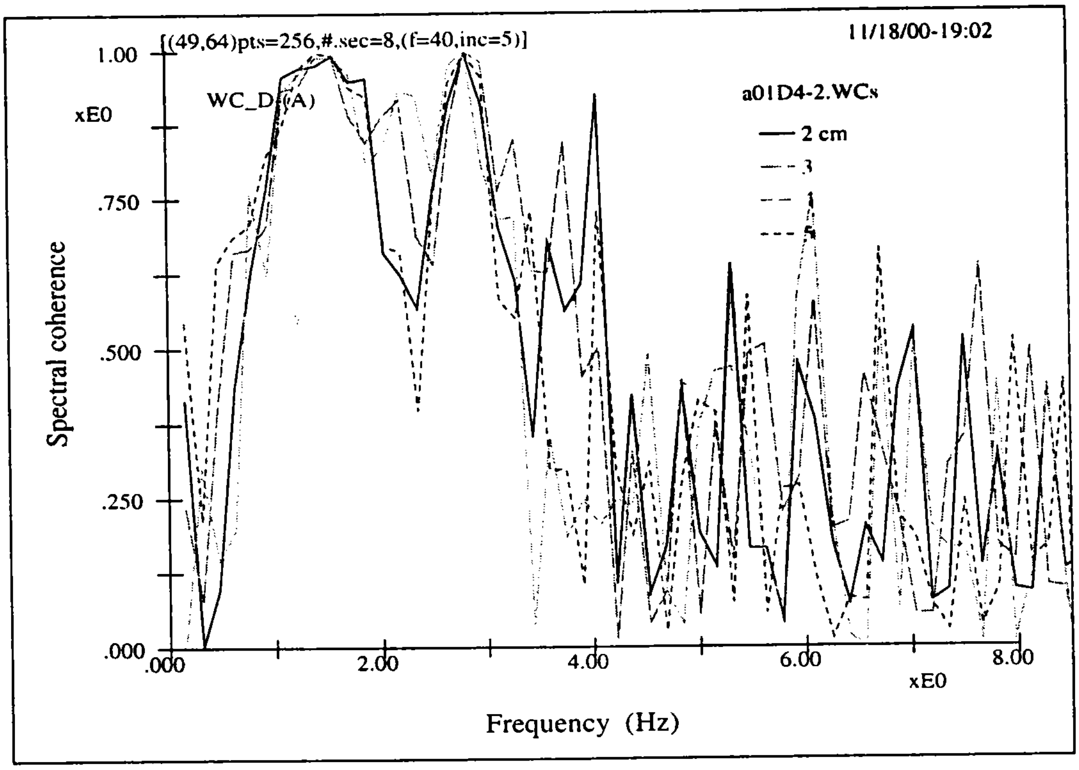

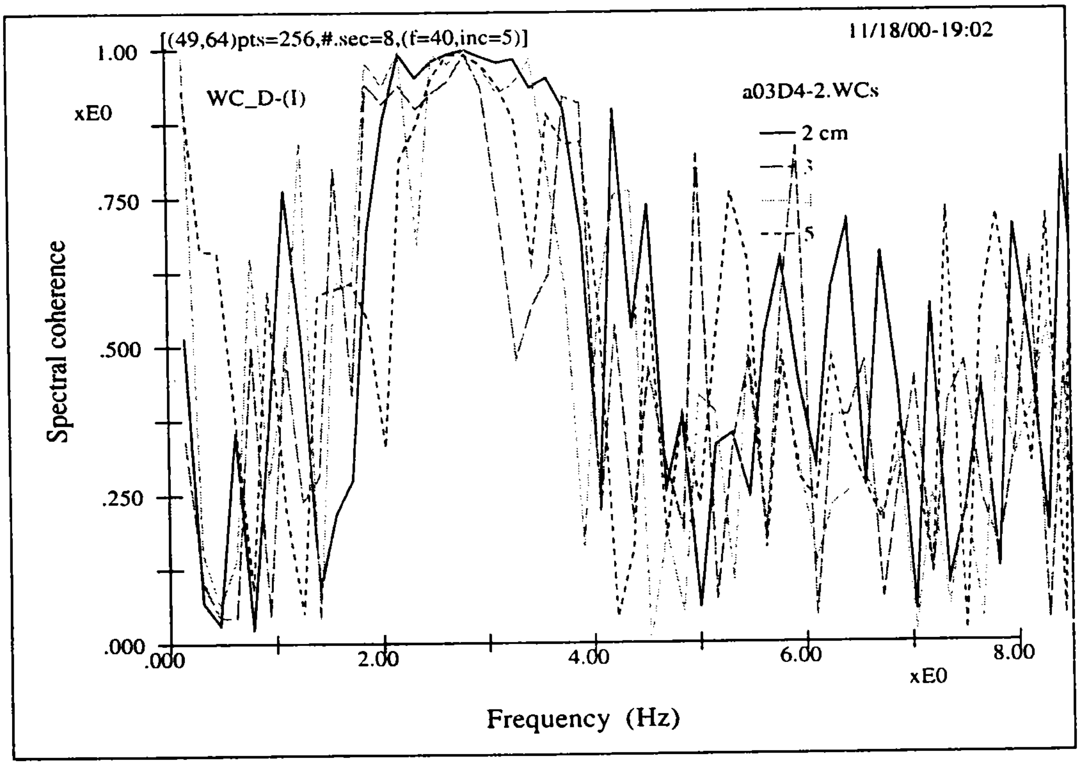

Figure 7.5: The spectral wave-current coherences for Stokes waves with wave steepness values of 0.06 (`top`) and 0.30 (`bottom`) — It is hard to infer any instability related feature.

Chapter 8

Phase Effect on Wavelet Coherence

8.1 The phase difference between wave and current

Until now all the coherences deal with surface waves and current in the gravitational direction, and the wave and current are measured at almost the same location. The basic water wave mechanics tells that there is a $\frac{\pi}{2}$ difference between the phases of surface displacement and water particle velocity in the gravitational direction, i.e., if the surface displacement $\eta \sim \cos\theta$, then the current speed $w \sim \sin\theta \sim \cos(\theta - \frac{\pi}{2})$. Therefore it warrants for us to check whether there is improvement in the wavelet wave-current coherence by further fine tuning one of the inner product projections.

8.2 A better shift-non-invariant property

To make such an adjustment both the carrier and the modulator of the Gaussian type wavelet need to be shifted; For all scales the phase of the carrier can easily be shifted to the left by simply making the $\frac{\pi}{2}$ adjustment, but the shift of the modulator must be calculated based on individual scale (a, or carrier frequency).

Figure 8.1 shows wavelet wave-current coherences with and without such a phase adjustment for the current speed. Obviously, the curves with or without the adjustment are almost identical, and this further indicates that the present wavelet coherence suffers from phase effects in a lesser degree than spectral coherence does, i.e, adverse effects due to shift-non-invariant property should be less critical for the used wavelet. ❖

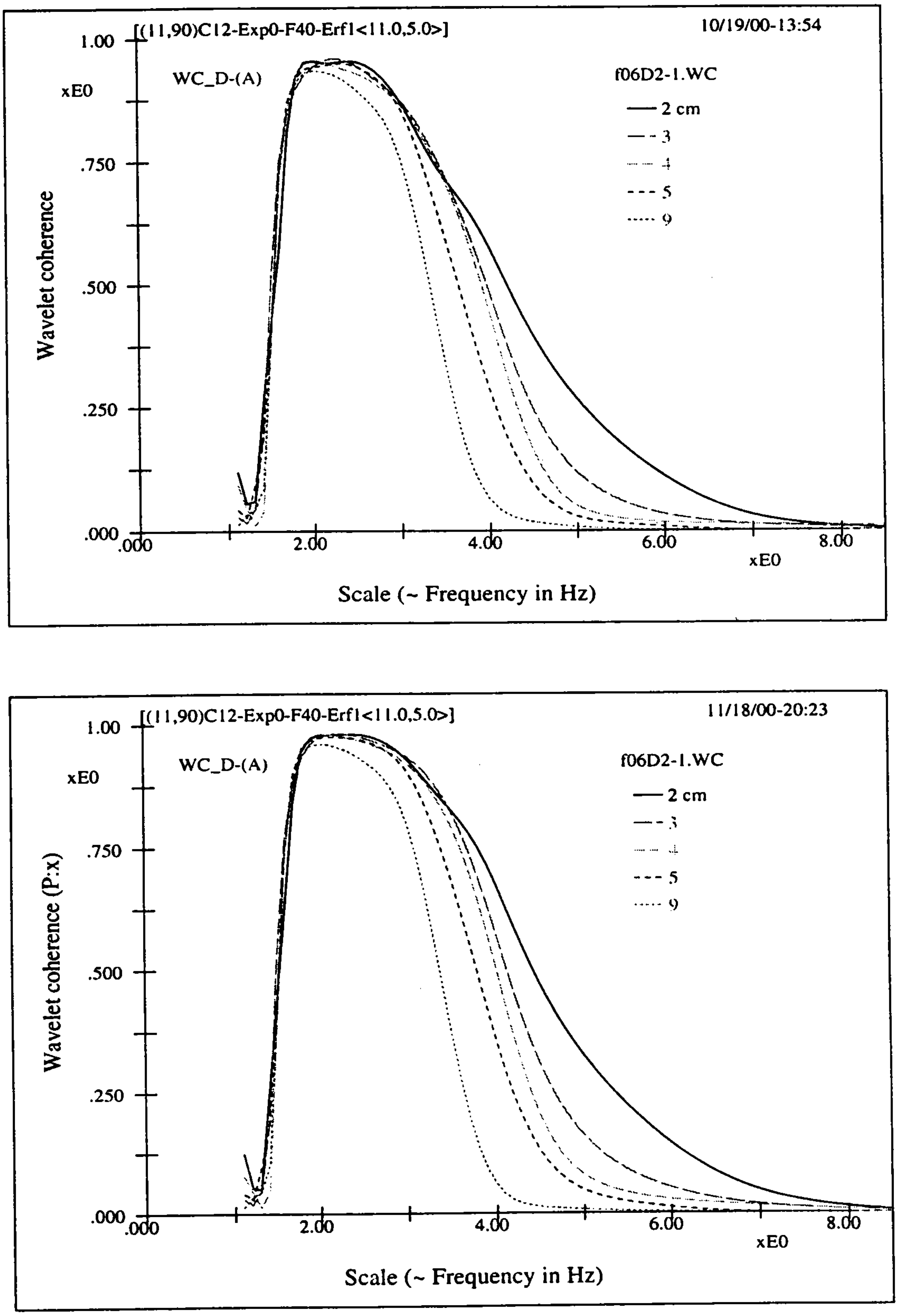

Figure 8.1: The wavelet wave-current coherences with (top) and without (bottom) the $\frac{\pi}{2}$ phase adjustment between surface wave and the vertical component of aqueous flow — The two figures are almost identical. The indication is that the wavelet coherence suffers from phase effects in a much lesser degree than does the spectral coherence, i.e., the used wavelet approach has a better shift-non-invariant property.

Chapter 9

Non-Concurrent or Displaced Measurements

9.1 Another form of phase effect

In the last chapter the subject is about phase; in this chapter what will be studied is also about phase. However, the previous chapter concerns the optimization of phase in which the phase shifts for the carrier waves are all fixed and their modulators are shifted according to individual scale sizes; and yet the present chapter concerns the effects of uncontrollable phase shifts that are associated with measurements acquired either non-concurrently or at two somewhat distantly spaced locations. Moreover, in the previous chapter the adjustment of phases is applied to the basis functions, but in the present chapter the phase noises are inherent in the target signals. Although, for cases of displaced but concurrent measurements, it might somewhat be possible to make the adjustments of the carrier waves and their modulators in a similar way to that of the previous chapter, the difference between phase speed and group velocity (energy propagation speed) complicates the matters. Furthermore, taking into account the support lengthes of short and long waves, one realizes that there is no consistent approach for all scales. As to non-concurrent measurements, there is simply no rule to make adjustment, not to mention those of wind wave cases.

9.2 Stokes wave cases with a small wave slope

Figure 9.1 shows both the wavelet and spectral coherences for non-concurrent measurements for a Stokes wave with a low wave slope of 0.06. The top and bottom sub-figures are respectively without and with the input of rain. From the wavelet coherence curves, it is clearly seen that this external input of rain has lowered the current-current coherence. And this is reasonable since at this low value of wave steepness the original wave and current fields should be relatively regular; therefore, an external disturbance reduces the coherences.

One additional point is that the coherence levels are not as high as those of concurrent measurements; nevertheless the peak values are still of relatively high magnitude when compared with other non-concurrent or any displaced measurements. As to the spectral coherence curves, the same wiggling exists and their peak values are mostly near unity.

9.3 Stokes wave cases with a large wave slope

Figure 9.2 shows both the wavelet and spectral coherences for non-concurrent measurements for a Stokes wave with a high wave slope of 0.30. The top and bottom sub-figures also show respectively cases without and with the input of rain. Here the interesting point for the wavelet coherence curves is the significant rises of coherence curves around the carrier frequency of 3 Hz. Without rain, due to the high instability of wave steepness of 0.03, the coherences are seen to be extremely low (below 0.2). But, when there is the action of rain, the impacts of rain drops neutralize the non-linearity and cause the reduction of randomness; henceforth the significant rises of coherences. Note that the flow measurement points for the present and the previous figures are the same and are located right behind the raining section. This phenomenon is compatible with the author's arguments in a study concerning the coupling mechanism of wind, wave and rain (Lee 1999b). In contrast, the corresponding spectral coherences curves are of noise with peak values also near to unity.

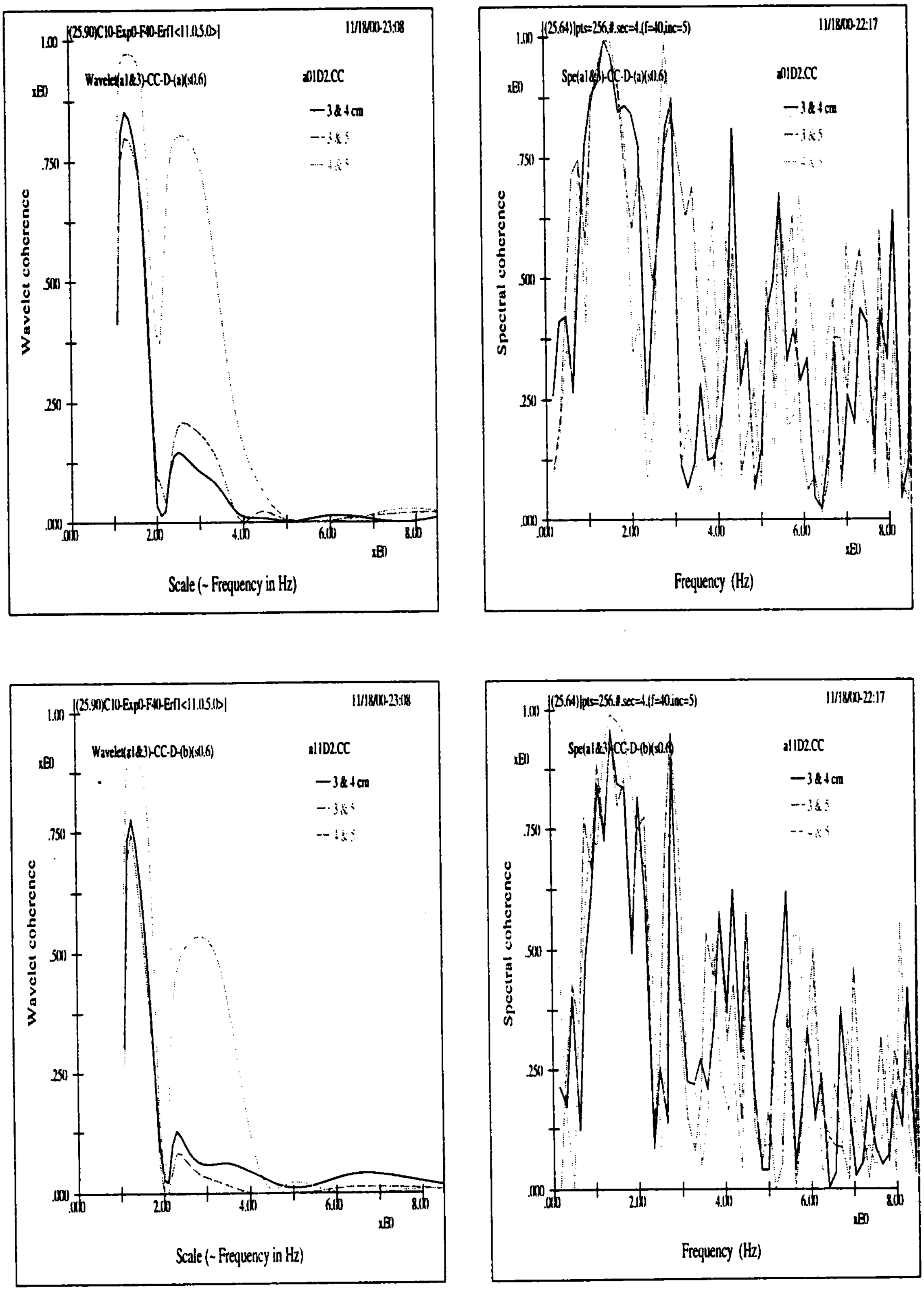

Figure 9.1: The wavelet (`right`) and spectral (`left`) coherences between current and current measured at different depthes as labeled in the figures for cases of non-concurrent measurements for a Stokes wave of low instability — Here a Stokes wave of a low wave steepness value of 0.06 without (`top`) and with (`bottom`) the influence of rain are shown.

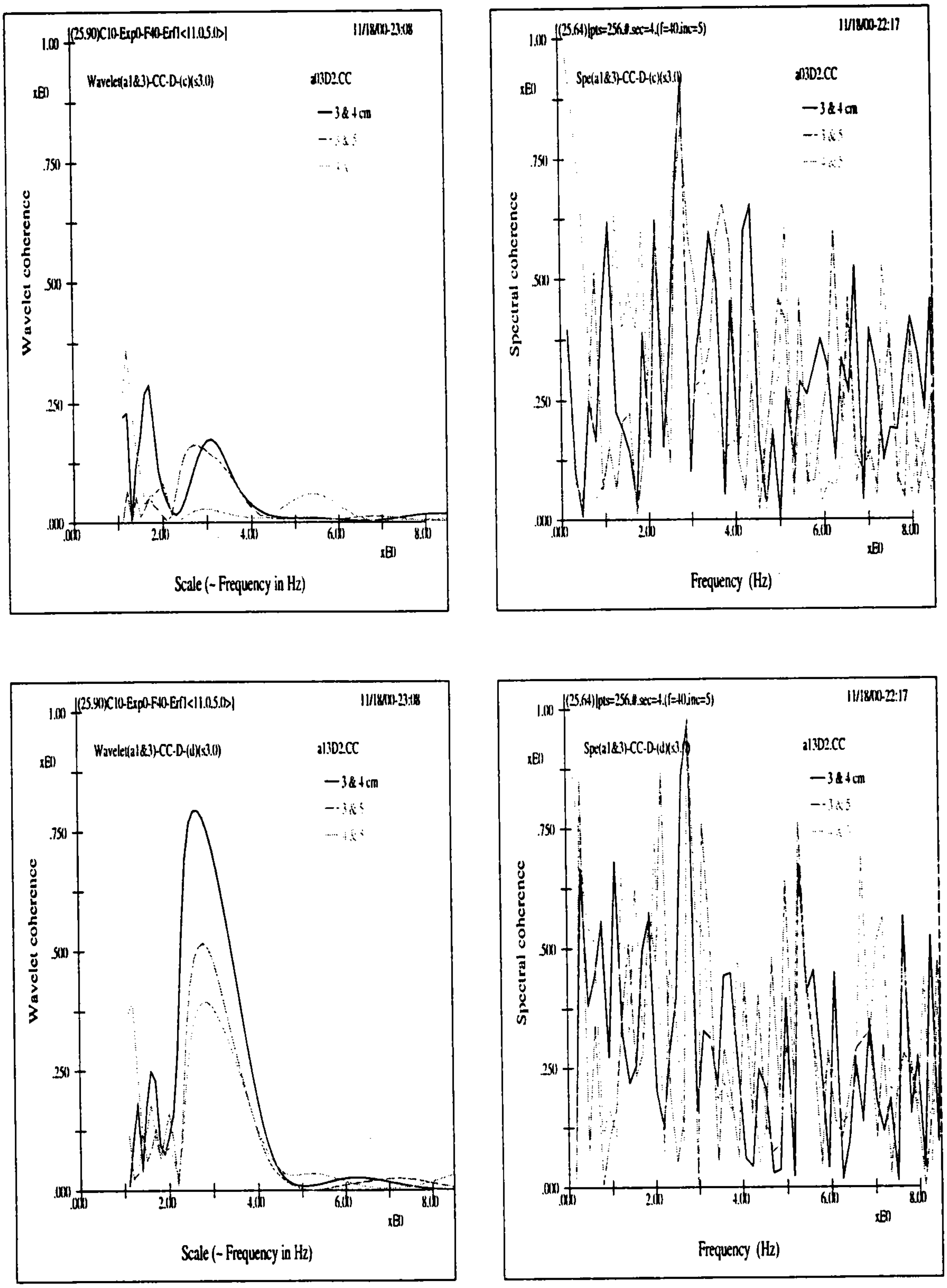

Figure 9.2: The wavelet (right) and spectral (left) coherences between current and current measured at different depthes as labeled in the figures for cases of non-concurrent measurements for a Stokes wave with a large wave steepness value of 0.30 — The sub-figures are without (top) and with (bottom) the influence of rain. Here the effects of the external input factor (i.e., the rain) on the instability, as identified by the wavelet coherences, manifests the interaction mechanism within a wind, wave and rain coupling system.

9.4 Wind wave cases

As to non-concurrent measurements for the wind wave cases shown in figure 9.3 it is seen that the coherence levels are very low (about 0.2) and no conclusive feature can be discerned, even though these current fields may be relatively stationary when viewed from wavelet's standpoint. It is of no doubt that randomized phases cause the problem. ❖

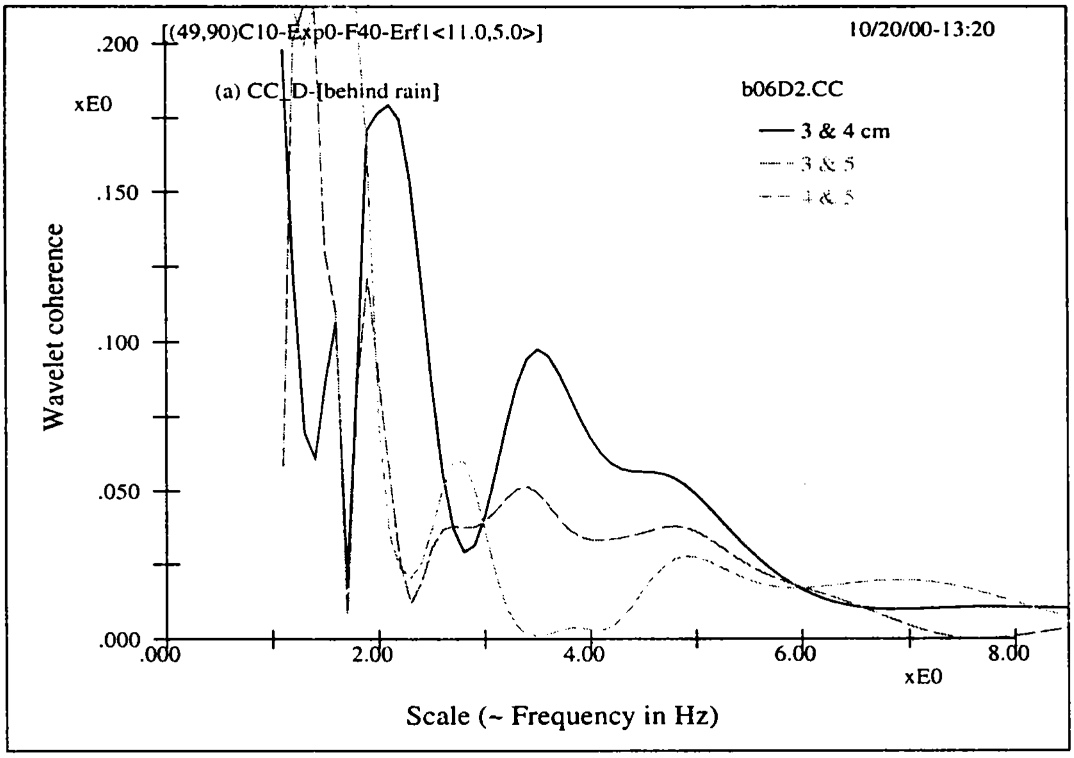

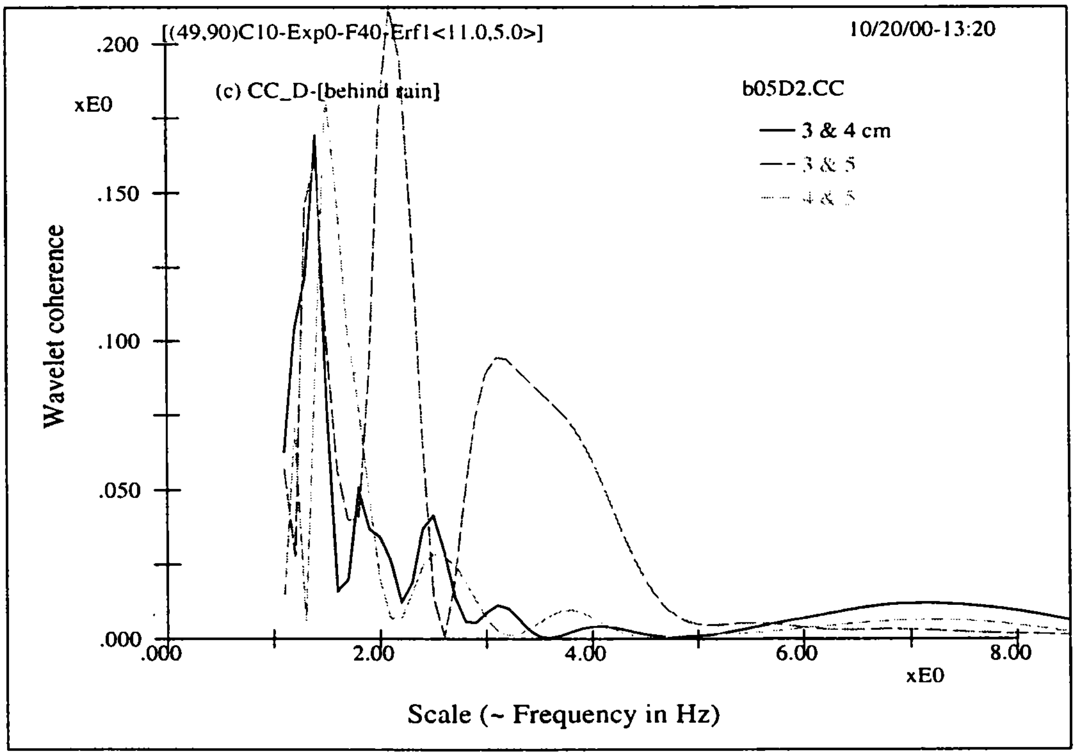

Figure 9.3: The wavelet coherences between current and current measured at different depthes for cases of non-concurrent measurements for two wind waves — Here wind waves of two wind speeds of 6.0 m/sec (`top`) and 5.1 (`bottom`) are shown.

Chapter 10

Complex and Real Coherences

10.1 Real and complex wavelets

The application formulae for wavelet coherence roots its soundness in the foundation of a strong theoretical background as stated in Chapter 2. As we know there basically exist infinitely many seeding functions (or mother wavelets), either of discrete or of continuous transform nature, that are able to furnish a complete (or lossless) wavelet reconstruction, i.e, to fulfill the law of resolution of identity. Furthermore, unlike Fourier domain where the basis functions are instinctively complex, the basis functions of wavelet can be either real or complex. And in fact commonly seen wavelets in various disciplines or applications are mostly real.

The continuous wavelet adopted here (equation 2.8) is a complex wavelet, and it is a natural extension of the identified optimum discrete wavelet, i.e., the semi-orthogonal cardinal spline wavelet. As we also know the optimum discrete Riesz wavelet is real, it therefore warrants for us to have a look at the coherences by using a function which is the real part of the complex modulated Gaussian wavelet and which, incidentally, is almost identical to the identified semi-orthogonal cardinal spline wavelet (Chui 1992a, b, c; Lee and Wu 1996a, b). Here the point of the statement is: even though the equation of resolution of identity (equation 2.5) requires that the function ψ be a wavelet, the use of such a real part function, though analytically being not a strict wavelet, should still satisfy the use of the equation.

10.2 Stokes wave cases

Figure 10.1 shows the complex and real wavelet wave-current coherences at individual depthes for the Stokes wave cases of 0.06 wave steepness. It is seen that the peak values of the real part wavelet coherences are somewhat lower than the complex ones and the band spreads of the peaks are also narrower. One additional feature is that the real wavelet coherences are generally further reduced for frequency bands of higher wave steepness, such as the second or higher harmonic band. Here the cause should be attributed to the fact that the local (or individual) wave steepness of higher harmonic band is of a higher magnitude and consequently of higher non-linear instability.

10.3 Wind wave cases

Figure 10.2 shows the complex and real wavelet wave-current coherences for aqueous flows measured at individual depthes for the cases of 6.0 m s^{-1} wind. It is seen that both the coherence levels and the shapes of curves are dramatically different. The peak values of the real wavelet coherences drop significantly and the trends among curves are not consistent. Here the indication is: local transient effects severely hamper the usefulness of a projection without phase information (i.e., taking an inner product with a real basis function). Alternatively speaking, without a complex operation, phase effects is much more critical, and a complex wavelet function basis helps to remove the harsh difference between synthesized wave forms composed of various component phases.

Another peculiar feature is: for complex wavelet coherences, the peak values are generally cluttering about unity, but, for real wavelet coherences, their peak values are generally differentiable. Moreover, the more transient (or more instability) the coherent field the lower the coherence level is (one can refer this argument to the figures shown in the

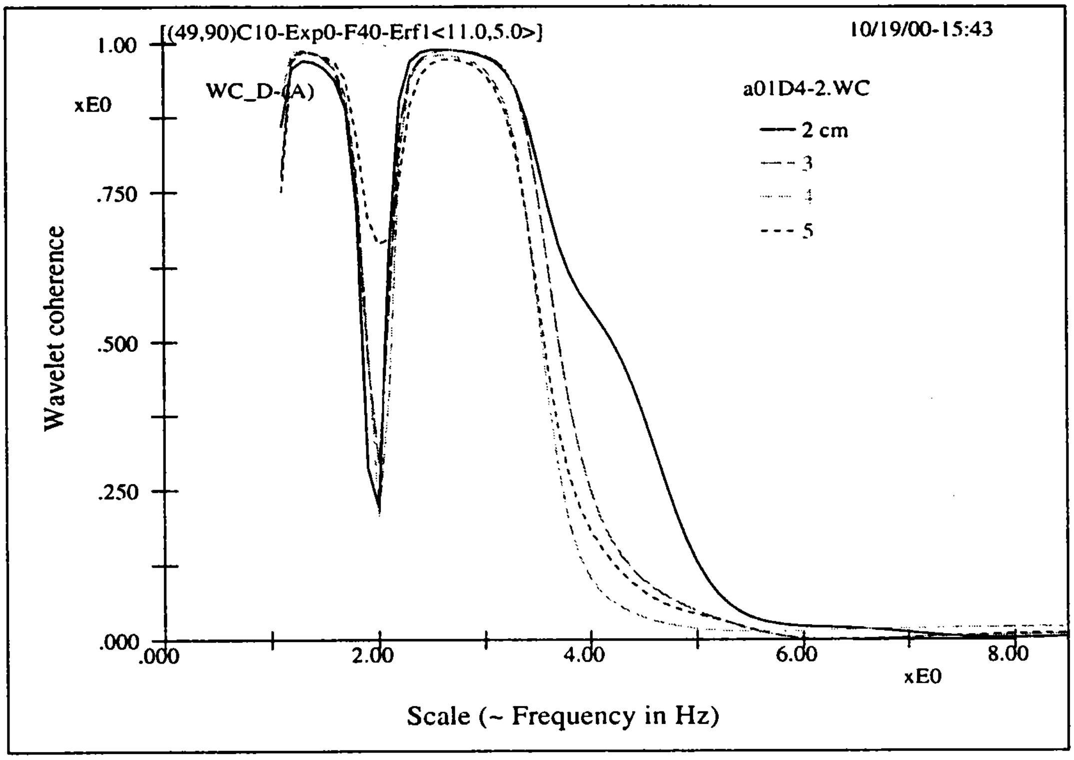

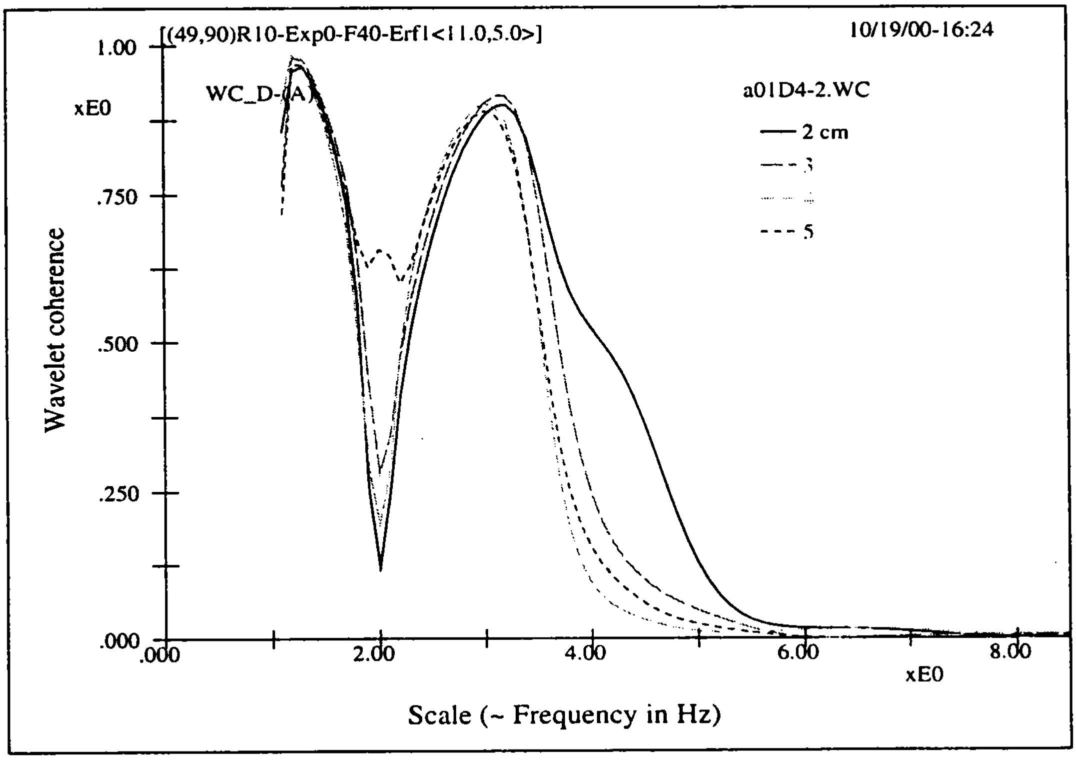

Figure 10.1: The complex (top) and real (bottom) wavelet wave-current coherences for aqueous flows measured at individual depthes for the Stokes wave cases of 0.06 wave steepness. It is seen that the peak values of the real part wavelet coherences are somewhat lower than the complex ones and the band spreads of the peaks are also narrower.

previous chapter too).

Overall, we conclude that the real wavelet coherence may also provide informative features for those conditions that are somewhat less transient or relatively more stationary. In this regard, the real wavelet coherences may sometimes serve as an index of instability or a pointer for unstable effects or randomness. Again, these functions cannot be facilitated by spectral coherences. ❖

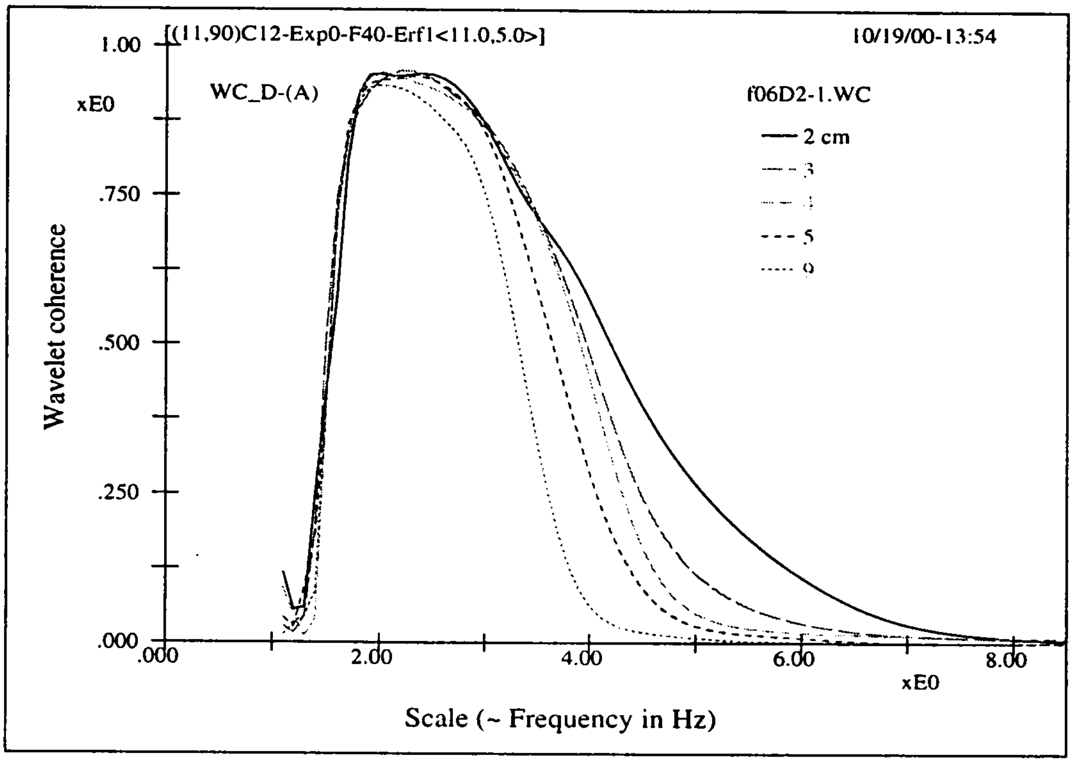

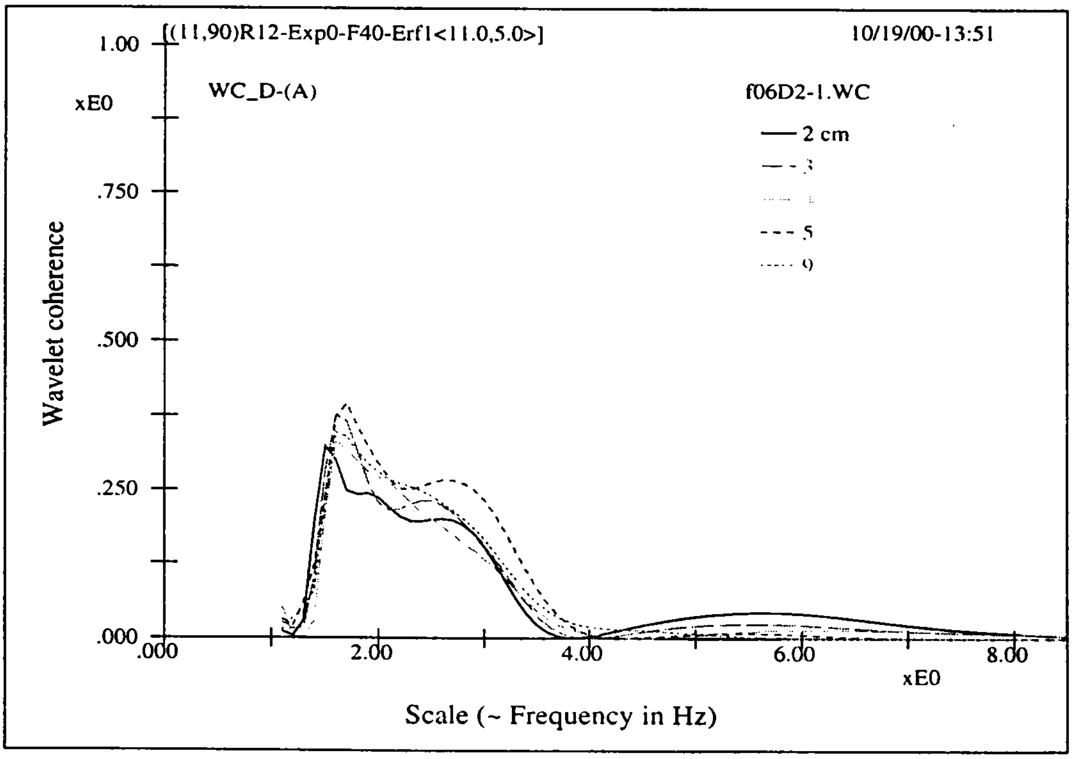

Figure 10.2: The complex (top) and real (bottom) wavelet wave-current coherences at individual depthes for wind wave cases. It is seen that the real part wavelet coherences are significantly lower than the complex wavelet coherences.

Chapter 11

Summary

We first outlined the main contents of two previous studies that laid the foundation for the successful applications of the present wavelet coherences. We then illustrated theoretical backgrounds for both spectral and wavelet coherences and discussed the different intimacy between their application formulae and exact analytic forms. And then all the rightfulness was vindicated by various informative topics centering on practical aspects of water wave lineaments. Results clearly show that the present wavelet coherence approach is far superior than that of the spectral coherence — either in extracting various features associated with multi-scale phenomena or in manifesting various water wave physics. Specifically, we show:

- The wavelet coherence approach is shown to yield features that are much less uncertain and far more distinguishable.
- The data length requirement is much more economic for the wavelet coherence approach. Apart form the fact that a few features can hardly ever be discerned using the spectral approach, the order difference in data length requirements is more than one.
- The wavelet coherence is able to identify micro phenomena embedded within macro signals. In particular, the existence of the natural frequency of the wind wave tank as well as its high order Stokes wave nature was identified using a single wave-

current measurement pair.

- The wavelet coherence is shown to be able to indicate the maturity of wind wave development, again, using only one single measurement pair.
- The wavelet coherence is shown to provide information related to a few innate physics, such as side band instability, Stokes wave features, influences of external inputs, etc.
- It is also shown that the wavelet coherence suffers less severely from the shift-non-invariant property.
- Not only the complex wavelet coherence, the real part wavelet coherence may also possibly yield informative features, especially for wave-current fields that are relatively less random or less transient.

Finally, let us summarize the properties that are inherent in the two methodologies and that cause the much differentiable performances between the two.

- Spectral coherence:
  - Forever-live waves do not tune to intimate physics
  - Limited number of coefficients (orthonormal)
  - Poor scale resolution (matching problem)
  - No control of frequency range (wasteful)
  - Serious ambiguity and phase noise
  - No adaption for better physics
  - More numerical noise
  - More artificial inputs
- Wavelet coherence:

- A more natural description using life-expectancy waves
- Much more abundant coefficients (residual)
- Unlimited scale resolution
- Focusing on scale range of interest (efficient)
- Time-scale window adaptations for better physics
- Fewer numerical noise
- Associated with an optimal function basis (Lee and Wu 96a, b)
- Both real and complex wavelets can be used
- ... Additional properties in contrast to those of spectral coherences (such as, having a formulation that is more closely related to background theory, no need of raw data segmentation, etc). ❖

REFERENCES

[1] Adrian, R. J. *Laser velocimetry*, chapter 5, pages 155–244. Hemisphere Publishing Corporation, New York, New York, USA, 1983.

[2] Aldroubi, A., and M. UNser. Families of wavelet transforms in connection with Shannon's Sampling Theory and the Gabor Transform. In C.K. Chui, editor, *Wavelets: A tutorial in Theory and Applications*, pages 509–528. Academic Press, Inc., San Diego, California, USA, 1992.

[3] Bracewell, B. *The Fourier Transform And Its Applications.* McGraw-Hill Book Company, Singapore, second edition, 1986.

[4] Brooke Benjamin, T. Instability of periodic wave trains in nonlinear dispersive systems. *Proc. Roy. Soc. Lond.*, A299:59–75, 1967.

[5] Brooke Benjamin, T., and J. E. Feir. The disintegration of wave trains on deep water. *J. Fluid Mech.*, 27:417–430, 1967.

[6] Brooke Benjamin, T., and J. J. Mahony. On the invariant property of water waves. *J. Fluid Mech.*, 49:385–389, 1971.

[7] Chui, C. K. *An Introduction to Wavelets.* Academic Press, Inc., San Diego, California, USA, 1992.

[8] Chui, C.K.. *Wavelets: A Tutorial in Theory and Applications.* Academic Press, Inc., San Diego, California, USA, 1992.

[9] Chui, C.K. On cardinal spline-wavelets. In M. B. Ruskai, G. Beylkin, R. Coifman, I. Daubechies, S. Mallat, Y. Meyer, and L. Raphael, editor, *Wavelets and Their Applications*, pages 439–452. Jones and Bartlett Publishers, Boston, New York, USA, 1992.

[10] Cohen, L. *Time-Frequency Analysis.* Prentice Hall PTR, Englewood Cliffs, New Jersey, USA, 1995.

[11] Coifman, R., Y. Meyer, and M.V. Wickerhauser. Size properties of wavelet packets. In M. B. Ruskai, G. Beylkin, R. Coifman, I. Daubechies, S. Mallat, Y. Meyer, and L. Raphael, editor, *Wavelets and Their Applications*, pages 453–470. Jones and Bartlett Publishers, Boston, New York, USA, 1992.

[12] Coifman, R., Y. Meyer, and M.V. Wickerhauser. Wavelet analysis and signal processing. In M. B. Ruskai, G. Beylkin, R. Coifman, I. Daubechies, S. Mallat, Y. Meyer, and L. Raphael, editor, *Wavelets and Their Applications*, pages 153–178. Jones and Bartlett Publishers, Boston, New York, USA, 1992.

[13] Coifman, R., Y.Meyer, and M.V. Wickerhauser. Entropy-based algorithms for best basis selection. *IEEE Tran. on Inform. Theory*, 38:713–718, 1992.

[14] Daubechies, I. Orthonormal bases of compactly support wavelets. *Communications on Pure and Applied Mathematics*, 41:909–996, 1988.

[15] Daubechies, I. *Ten Lectures on Wavelets.* SIAM, Philadelphia, USA, 1992.

[16] Debnath, L. *Nonlinear Water Waves.* Academic Press, Inc., San Diego, California, USA, 1994.

[17] Feidhtingger, H.G., and K. Gröchenig. Gabor wavelets and the Heisenberg group: Gabor expansion and short time Fourier transform from the group theoretical point of view. In C.K. Chui, editor, *Wavelets: A tutorial in Theory and Applications*, pages 359–397. Academic Press, Inc., San Diego, California, USA, 1992.

[18] Feidhtingger, H.G., and K. Gröchenig. Non-orthogonal wavelet and Gabor expansions and group representations. In M. B. Ruskai, G. Beylkin, R. Coifman, I. Daubechies, S. Mallat, Y. Meyer, and L. Raphael, editor, *Wavelets and Their Applications*, pages 353–376. Jones and Bartlett Publishers, Boston, New York, USA, 1992.

[19] Gabor, D. Theory of communication. *Journal of the IEE*, 93:429–457, 1978.

[20] Greenberg, M.D. *Advanced Engineering Mathematics.* Prentice Hall PTR, Englewood Cliffs, New Jersey, USA, 1988.

[21] Hasselmann, K. On the nonlinear energy transfer in a gravity wave spectrum. *J. Fluid Mech.*, 12:481–500, 1962.

[22] Lake, B.M., and H.C. Yuen. A note on some nonlinear water wave experiments and comparison of data with theory. *J. Fluid Mech.*, 83:75–81, 1977.

[23] Lake, B.M., and H.C. Yuen. A new model for nonlinear gravity waves, Part 1, Physical model and experimental evidence. *J. Fluid Mech.*, 88:33–62, 1978.

[24] Lake, B.M., H.C. Yuen, H. Rundgaldier, and W.E. Ferguson. Nonlinear deep-water waves: Theory and experiment, Part 2, Evolution of a continuous wave train. *J. Fluid Mech.*, 83:49–74, 1977.

[25] Lamb, H. *Hydrodynamics*. Cambridge University Press, Cambridge, England, sixth edition, 1932.

[26] Lee, Y.R. Signal analysis from wave modulation perspective – Part I: Characterizing the analytic signal procedure. Technical report, No.1997–7, Institute of Harbor and Marine Technology, Taichung, Taiwan, 1997.

[27] Lee, Y.R. *Interaction Scales in a Wind, Wave, and Rain Coupling System*. Ph.d. dissertation, University of Delaware, Newark, Delaware, Nov. 1999.

[28] Lee, Y.R., and J. Wu. Continuous wavelet transform using a locally adapted time-frequency window. In *Proc. 18th Conf. on Coastal Engineering in Taiwan*, pages 95–106, 1996.

[29] Lee, Y.R., and J. Wu. Wavelet and wavelet packet best basis for laboratory water waves. In *Proc. 18th Conf. On Coastal Engineering in Taiwan*, pages 83–94, 1996.

[30] Lee, Y.R., and J. Wu. Time-frequency features and side band instability. In *Proc. 19th Conf. On Coastal Engineering in Taiwan*, pages 32–39, 1997.

[31] Lee, Y.R., and J. Wu. Fourier perspectives of rain's effects on surface waves. *Proc. 22th Conf. on Coastal Engineering in Taiwan*, pages 59–66, 2000.

[32] Lighthill, M.J. Some special cases treated by Whitham theory. *Proc. Roy. Soc. Lond.*, A299:38–53, 1967.

[33] Liu, P. Wavelet spectrum analysis and ocean wind waves. In E.F. Georgiou, editor, *Wavelets in Geophysics*, pages 151–166. Academic Press, Inc., San Diego, California, USA, 1994.

[34] Longuet-Higgins, M.S. The instability of gravity waves of finite amplitude in deep water I, Superharmonics. *Proc. Roy. Soc. Lond.*, A360:471–488, 1978.

[35] Longuet-Higgins, M.S. The instability of gravity waves of finite amplitude in deep water II, Subharmonics. *Proc. Roy. Soc. Lond.*, A360:489–505, 1978.

[36] Mallat, S. A theory for multiresolution signal decomposition: the wavelet representation. *IEEE Tran. on Pattern Anal. and Mach. Intel.*, 11:674–693, 1989.

[37] Mallat, S. *A Wavelet Tour of Signal Processing*. Academic Press, Inc., San Diego, California, USA, 1998.

[38] Mallat, S., and S. Zhong. Wavelet transform maxima and multiscale edges. In M. B. Ruskai, G. Beylkin, R. Coifman, I. Daubechies, S. Mallat, Y. Meyer, and L. Raphael, editor, *Wavelets and Their Applications*, pages 67–104. Jones and Bartlett Publishers, Boston, New York, USA, 1992.

[39] Massopust, P.R. *Fractal Runctions, Fractal Surfaces, and Wavelets*. Academic Press, Inc., San Diego, California, USA, 1994.

[40] Melville, W. K. The instability and breaking of deep water waves. *J. Fluid Mech.*, 115:165–185, 1982.

[41] Melville, W. K. Wave modulation and breakdown. *J. Fluid Mech.*, 128:489–506, 1983.

[42] Meyer, Y. *Wavelets and operators*. Cambridge University Press, New York, USA, 1992.

[43] Poon, Y.K., S. Tang, and J. Wu. Interaction between rain and wind waves. *J. Phys. Oceanogr.*, 22:977–987, 1992.

[44] Press, W. H., S. A. Teukolsky, W. T. Vetterling and B. P. Flennery. *Numerical Recipes in Fortran*. Cambridge University Press, New York, USA, second edition, 1992.

[45] Soumekh, M. *Fourier Array Imaging*. Prentice Hall, Inc., Englewood Cliffs, New Jersey, USA, 1994.

[46] Stuart, J.T., and R.C. DiPrima. The Eckhaus and Benjamin-Feir resonant mechanisms. *Proc. Roy. Soc. Lond.*, A362:27–41, 1978.

[47] Su, M.Y. Evolution of groups of gravity waves with moderate to high steepness. *Phys. Fluids*, 25:2167–2174, 1982.

[48] Tchamitchian, Ph., and B. Torresani. Ridge and skeleton extraction from the wavelet transform. In M. B. Ruskai, G. Beylkin, R. Coifman, I. Daubechies, S. Mallat, Y. Meyer, and L. Raphael, editor, *Wavelets and Their Applications*, pages 123–151. Jones and Bartlett Publishers, Boston, New York, USA, 1992.

[49] Whitham, G. B. Nonlinear dispersion of water waves. *J. Fluid Mech.*, 27:399–412, 1967.

[50] Wickerhauser, M.V. Acoustic signal compression with wavelet packets. In C.K. Chui, editor, *Wavelets: A tutorial in Theory and Applications*, pages 679–700. Academic Press, Inc., San Diego, California, USA, 1992.

[51] Wickerhauser, M.V. Comparison of picture compression methords: wavelet, wavelet packet, and local cosine. In C. K. Chui, editor, *Wavelets: Theory, Algorithms, and Applications*, pages 585–621. Academic Press, Inc., San Diego, California, USA, 1994.

[52] Wu, J. Wind-induced drift currents. *J. Fluid Mech.*, 68:49–70, 1975.

[53] Yuen, H. C., and B. M. Lake. Nonlinear deep water waves: Theory and experiment. *Phys. Fluids*, 18:956–960, 1975.

[54] Zhang, X. Wavenumber spectrum of very short wind waves: An application of two dimensional Slepian windows to spectral estimation. *J. of Atmospheric and Oceanic Technology*, 11:489–505, 1994.

國家圖書館出版品預行編目（CIP）資料

Wave Characterizations Using Wavelet and Spectral Coherences
（子波型與波譜型共關頻振特性比較研究）

著　　者：李勇榮
出版機關：交通部運輸研究所港灣技術研究中心
地　　址：台中縣梧棲鎮臨海路83號 (43501)
網　　址：www.ihmt.gov.tw
電　　話：04-26564216
出版日期：中華民國八十九年十二月
印刷單位：明昌文具印刷行
地址：台中縣梧棲鎮梧北路142號
電話：04-26563150
版次冊數：初版一刷110冊
工本售價：350 元
展售地點：台中縣梧棲鎮臨海路83號　電話：04-26564216

GPN: 009254890340